

专题——微弧氧化在腐蚀领域中的应用

微弧氧化涂层微纳米孔调控及 功能化应用研究进展

王树棋, 王亚明, 邹永纯, 陈国梁, 王钊, 欧阳家虎, 贾德昌, 周玉

(哈尔滨工业大学 a.材料科学与工程学院 特种陶瓷研究所 b.先进结构功能一体化材料
与绿色制造技术工业和信息化部重点实验室, 哈尔滨 150001)

摘要: 从膜层特征孔结构形成的基本原理、影响因素和控制策略以及功能性陶瓷涂层设计制备的角度, 综述了微弧氧化工艺调控多级微纳米孔结构的最新研究进展。从微纳米孔产生的本质与形成机理出发, 阐述了微纳米孔结构的分类以及表征方法。在综述电解液成分、电源模式以及电参数对微纳米孔的尺寸、形状以及分布的影响基础上, 从微纳米孔的构建、消减(甚至消除)和利用角度, 给出了微弧氧化涂层多级微纳米孔的调控策略, 进而讨论了如何构建适应不同应用服役环境下的特殊功能化涂层。此外, 探索了微纳米孔结构调控的新途径, 并给出了未来发展的研究方向。

关键词: 微弧氧化; 功能化涂层; 微纳米孔; 结构调控

中图分类号: TG174.4 **文献标识码:** A **文章编号:** 1001-3660(2021)06-0001-22

DOI: 10.16490/j.cnki.issn.1001-3660.2021.06.001

Generation, Tailoring and Functional Applications of Micro-Nano Pores in Microarc Oxidation Coating: A Critical Review

*WANG Shu-qi, WANG Ya-ming, ZOU Yong-chun, CHEN Guo-liang,
WANG Zhao, OUYANG Jia-hu, JIA De-chang, ZHOU Yu*

(a. Institute for Advanced Ceramics, School of Materials Science and Engineering, b. Key Laboratory of Advanced Structural-Functional Integration Materials & Green Manufacturing Technology, Harbin Institute of Technology, Harbin 150001, China)

ABSTRACT: The research progress of microarc oxidation process to tailor hierarchical micro-nano pores is reviewed from the views of scientific mechanism, influencing factors, control strategies and design preparation of functional ceramic coatings. Based on the nature and formation mechanism of micro-nano pores, the classification and characterization methods of micro-nano pore structures are described. After reviewing the influence of electrolyte composition, power supply mode and electrical

收稿日期: 2021-04-19; 修订日期: 2021-05-11

Received: 2021-04-19; Revised: 2021-05-11

基金项目: 国家自然科学基金(52071114, 52001100, 51571077, 51371071, 50701014, 60776803); 国家自然科学基金创新研究群体(51621091); 中国航空科学基金(20163877014)

Fund: Supported by National Natural Science Foundation of China (52071114, 52001100, 51571077, 51371071, 50701014, 60776803); Innovative Research Groups of the National Natural Science Foundation of China (51621091); Aviation Science Foundation of China (20163877014)

作者简介: 王树棋(1994—), 男, 博士研究生, 主要研究方向为微弧氧化涂层。

Biography: WANG Shu-qi (1994—), Male, Doctor student, Research focus: microarc oxidation coating.

通讯作者: 王亚明(1978—), 男, 博士, 教授, 主要研究方向为微弧氧化涂层。邮箱: wangyaming@hit.edu.cn

Corresponding author: WANG Ya-ming (1978—), Male, Doctor, Professor, Research focus: microarc oxidation coating. E-mail: wangyaming@hit.edu.cn

引文格式: 王树棋, 王亚明, 邹永纯, 等. 微弧氧化涂层微纳米孔调控及功能化应用研究进展[J]. 表面技术, 2021, 50(6): 1-22.

WANG Shu-qi, WANG Ya-ming, ZOU Yong-chun, et al. Generation, tailoring and functional applications of micro-nano pores in microarc oxidation coating: A critical review[J]. Surface technology, 2021, 50(6): 1-22.

parameters on the size, shape and distribution of micro-nano pores, the strategies on how to tailor hierarchical micro-nano pores are proposed from the aspects of construction, reduction (or even elimination) and utilization of micro-nano pores. Furthermore, how to construct special functional coatings suitable for different service environments is further discussed. Finally, the latest process exploration for tailoring the micro-nano pore structure and possible developing trends is presented.

KEY WORDS: microarc oxidation; functional coatings; micro-nano pores; structural tailoring

微弧氧化 (Microarc Oxidation, MAO) 技术, 又称等离子体电解氧化 (Plasma Electrolytic Oxidation, PEO) 技术^[1], 是在金属 (铝、镁、钛、锆、铌、钽合金等) 及其复合材料上施加电压, 使金属表面绝缘膜发生介质击穿, 产生微弧放电, 在放电微区的局部高温高压和电场等作用下, 使金属表面发生氧化, 进而在基体金属表面形成以基体金属氧化物为主、电解液所含成分参与改性的具有特定组成与结构的功能化陶瓷涂层^[2-4]。

微弧氧化技术工艺简单, 安全环保, 重要的是涂层结构与功能特性的可设计性强, 可构建抗磨减摩、耐腐蚀、高温热防护、光学热控、介电绝缘、生物医用、催化、电池活性电极等一系列功能化涂层^[5-14]。由微弧氧化击穿放电的本质所决定, 微弧放电过程产生的放电通道不能完全封闭, 将在涂层与基体界面、涂层中间层或涂层表面残留微纳米孔。残留的微纳米孔^[15-19]分为: 界面孔, 其数量少, 尺寸小, 孔径在 100 nm 之内; 中间层孔, 其数量增加, 平均孔径为 300 nm; 表面孔, 其形貌多样, 孔径尺寸为 1~5 μm,

孔隙率为 5%~40%。揭示微弧火花放电诱导微纳米孔的形成机理, 进而调控微纳米孔尺寸、形状、空间分布状态, 势必影响涂层的基本物理与化学性能^[20-23], 包括力学性能 (强度、硬度、摩擦系数、结合力)、热学性能 (导热系数、热辐射)、电学性能 (介电绝缘性、半导体性)、电化学性能、生物学性能 (骨植人、生物相容性) 等。因此, 如何调控和利用微弧氧化涂层的微纳米孔, 以便按需设计并构建特定功能的陶瓷涂层, 是本领域的前沿课题, 也是重点和难点问题。

关于微弧氧化涂层微纳米孔结构调控与性能相关性的学术论文统计结果如图 1 所示。由图 1a 可见, 自 2005 年以来, 与微弧氧化涂层微纳米孔相关的研究论文数量呈快速增加的趋势。由图 1b 可见, 涂层微纳米孔结构调控以及功能性应用研究主要集中在抗腐蚀、抗磨减摩、生物活性涂层等, 而热防护、光学热控、绝缘介电、催化、电池活性电极等新型功能化涂层相关研究亦有增加趋势。由此可见, 微弧氧化涂层多级微纳米孔生成控制及功能化应用研究, 是表面技术领域持续关注的热点。

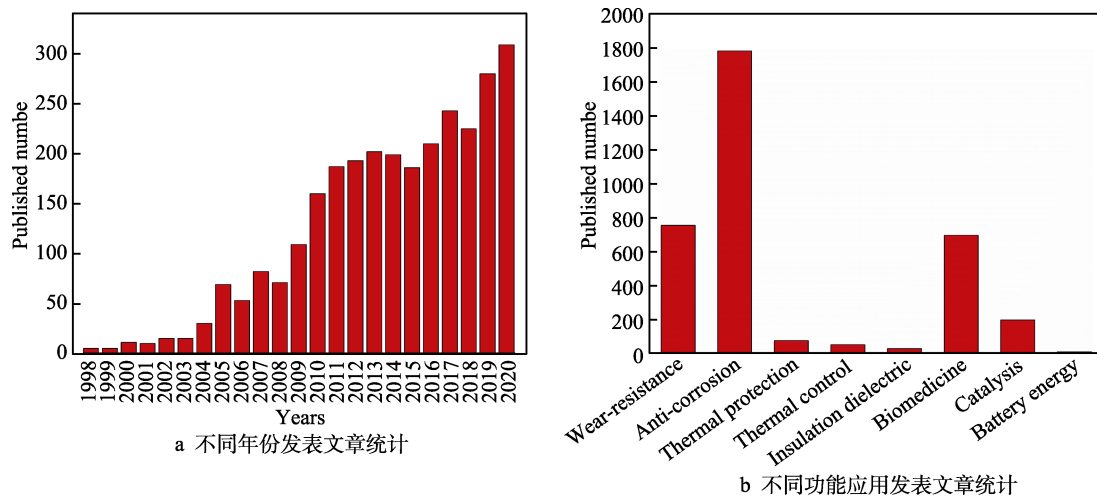


图 1 与微弧氧化涂层微纳米孔相关研究学术论文统计 (来源于 Web of Science 数据库)

Fig.1 The distribution of papers for (a) related study of micro-nano pores in MAO coating, (b) multifunctional applications (from the Web of Science database)

本文旨在从微弧氧化涂层多级微纳米孔形成的过程机理出发, 在综述电解液成分、电源模式、电参数对微纳米孔的尺寸、形状、分布的影响的基础上, 拟给出微弧氧化涂层多级微纳米孔的调控策略, 进而讨论如何构建适应不同应用服役环境的特殊功能化涂层。此外, 本文探索了微纳米孔结构调控的新途径, 并给出未来发展的研究方向。

1 涂层中微纳米孔形成机理、分类及表征

1.1 微纳米孔形成的基本过程

微弧氧化涂层的生长, 伴随着气泡产生、火花放电及组织结构演变的过程, 大致可划分为氧化初期阻

挡层的形成、介质击穿、放电通道形成。通道内基底金属反应生成氧化物，在高温、高压以及电场等作用下，熔融物喷射-冷却-凝固-相变，通常形成内层致密和外层疏松多孔的结构^[24-26]。学者们主要针对火花放电的本质，提出相应的微弧氧化机理模型，如析氧反应下的电子“雪崩”^[27]、定量的电子隧道效应机理^[28-29]、微弧氧化电压和涂层生长关系^[30]、火花沉积过程^[31]及自由电子和辉光放电^[32]等模型，研究分析涂层组织结构与基底/涂层/电解液界面化学反应的关系，进而建立微纳米孔结构生长模型。微弧氧化涂层微纳米孔形成的基本过程与机理，主要集中在以下方面。

金属电极在施加外电压作用下，金属表面介质层失稳—击穿放电—形成贯穿通道，而贯穿涂层的通道类似一个个微电桥，电解液容易进入通道，将基体正极与电源负极连通，电流从这些贯穿膜层的通道中流过，产生火花放电。火花放电产生的熔融产物冷却凝固后，作为涂层成分堵塞通道，残留的未封闭通道形成微纳米孔结构。电子“雪崩”效应下产生的电子在外加强电场下，通过电解液进入微弧氧化膜层，引起膜层介电击穿，产生等离子体放电，形成放电通道，从而产生微纳米孔。孔内微放电是由涂层/电解液界面或涂层中微孔的气体放电产生的，这可能是由于微孔底部阻挡层的初始介电击穿引起，导致涂层不断生长，并持续形成微纳米孔。放电击穿过程中，微区瞬间高温烧结形成熔融物，等离子体放电使内部熔融氧

化物聚集，并向外逸出，迅速冷却凝固后，使涂层形成不同形貌的微纳米孔^[33]。在微弧氧化过程中，火花放电并形成放电通道，使氧气向外析出并释放，引起微弧氧化涂层孔洞的产生^[19,34]，并形成“火山口状”的组织特征，在涂层表面上可明显观察到孔洞存在。

由此可见，由于微弧氧化过程中涉及的反应复杂，包括电化学、热化学、热学、等离子体物理学等，已经建立的微纳米孔结构机理模型存在一定的局限性，通常只能在特定环境下（特定过程中）解释某种单一因素的作用效果。因此，明确等离子体放电的微观作用机制，综合考虑在整个涂层生长过程中诸多影响因素，建立统一完善的微纳米孔结构形成模型，仍然是当前研究的热点。近几年，在上述微纳米孔结构生长模型的基础上，研究人员从熔凝机制、火花放电、气体释放及电解液选择性溶解等方面进一步揭示了微纳米孔结构的形成原理。

在放电诱发反复熔凝过程中，放电通道内形成的熔融产物瞬间快速冷却，形成不同结构的纳米晶或非晶态组织。Wang Y. M. 等^[35]结合微弧氧化涂层的微纳米孔组织结构演变以及与基体、电解液界面复杂的等离子化学反应，提出了击穿-通道-熔凝效应与陶瓷涂层形成机理模型。利用透射电镜等先进表征手段，发现在基体和涂层之间存在的界面层，由不同结构的纳米晶或非晶态组织组成。同时在放电通道周围形成瞬时温度梯度，导致放电通道形成残留放电微纳米孔^[24]，在微纳米孔边缘生成柱状晶组织（如图 2 所示）^[36]。

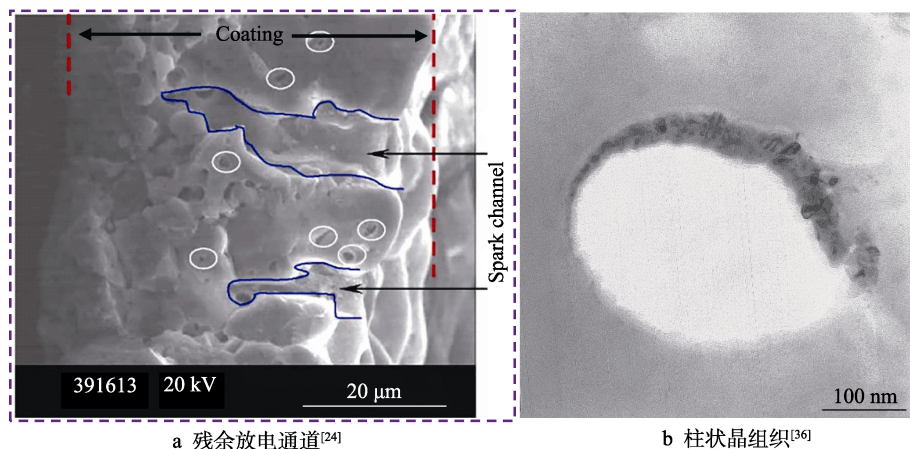


图 2 放电结束后涂层中残留的放电微纳米孔及其边缘柱状晶组织

Fig.2 Micro-nanopores and columnar crystal around pores in the coating after spark decaying: a) remained spark channels^[24]; b) columnar crystal around pores^[36]

R. O. Hussein 等^[37]利用光发射谱技术（Optical emission spectroscopy, OES），提出了 3 种等离子体放电模型（如图 3a 所示），以揭示微弧氧化不同层结构中微纳米孔的形成原因：微弧氧化涂层表面放电（A 型）、金属/氧化物界面放电（B 型）、微弧氧化膜表层下的中间孔结构内部放电（C 型）。由放电形成的不同物质，在涂层表面处明显表现为不同形态，并

分别对应不同微纳米孔结构（薄煎饼状、结节状等）。Cheng Y. L. 等^[38]在上述 3 种放电类型的基础上，增加另外 2 种放电模式（如图 3b 所示），进一步拓展了等离子体放电模型和微纳米孔形成机理。其中，D 型为涂层/基体处孔隙底部产生的放电，E 型表示发生在部分剥离的微弧氧化膜表层的放电。结果表明，不同类型放电导致不同微纳米孔形貌的形成，并在这些微纳

米孔中形成等离子体放电，进一步促进涂层厚度增加和复杂孔结构演变。Xue W. B. 等^[39-40]在研究微纳米孔形成过程中，提出每个放电火花都击穿氧化层，并形成等离子体放电通道，从而使离子电流、电子电流以及氧化膜层熔融电流的导通，放电模型如图 4 所示。不同类型的放电火花，形成不同结构的微纳米孔。虽

然这些火花放电机制提供了在电极界面处可能发生的放电行为和涂层微纳米孔结构生长模型，但并非所有方法都适用于每个微弧氧化过程。这需要进一步的实验证据来区分这些机制，并确定它们在涂层生长和微纳米孔形成过程中的主导地位。

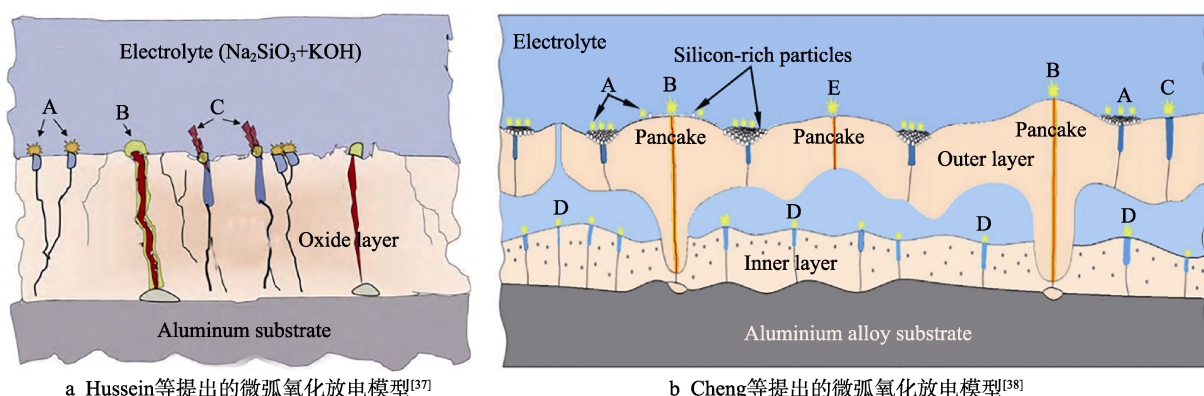


图 3 微弧氧化过程中的等离子体放电模型^[37]

Fig.3 Schematic diagram of the plasma discharge during MAO process: a) schematic illustrations of the discharge types according to the model proposed by Hussein et al.^[37]; b) schematic illustration of the discharges model described by Cheng for the MAO coating^[38]

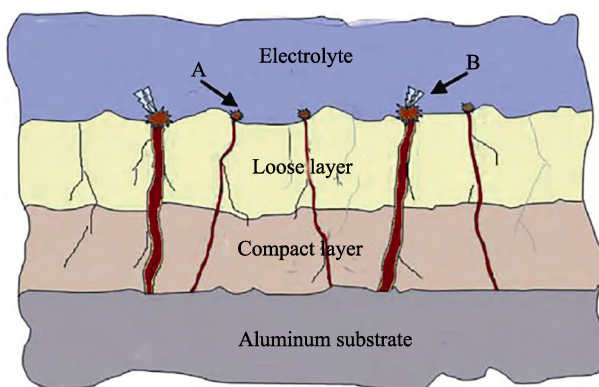


图 4 微弧氧化过程中的等离子体放电模型^[39]

Fig.4 Schematic illustration of the plasma discharge during MAO process^[39]

在等离子体放电通道形成微纳米孔的前提下，气体的析出和释放也可能引起涂层微纳米孔结构的形成和变化^[19,34]。在高温高压下，微区持续放电，涂层中形成放电通道，熔融氧化物中溶解氧的浓度显著增加，而且在放电过程中，产生的氧气很可能被滞留在局部放电附近的熔融氧化层中。当熔融物迅速冷却时，氧气释放，并通过氧化层流通、逃逸，从而形成细小连通的微纳米孔洞。随着氧化时间的增加，涂层不断增厚，火花在涂层缺陷处持续放电击穿，进一步导致微纳米孔洞和裂纹在薄弱、缺陷部分产生，并可能形成网状交联区域以及蠕虫状的凸起，其中凸起区域和凹陷区域交错纵横。

双脉冲模式下，在阴极极化过程中的不同阶段，阴极放电以及涂层表面气体演化行为，也可能导致微

纳米孔结构生长和形貌发生改变。最近发展的“软火花”放电模式（如图 5 所示）^[41-43]，表现为阳极电压降低、瞬态电流-电压曲线滞后、声发射降低以及等离子体放电在基体表面分布更加均匀等特征，能有效避免产生大而贯穿的孔结构，有助于形成厚而致密的涂层。

此外，电解液成分对涂层表面微纳米孔结构形成过程的影响，特别是选择性溶解作用，也备受关注。Li 等^[44]通过调节电解液成分，利用四硼酸盐强的化学溶解性，调控出不同于传统“火山口状”的“cortex-like”复合双尺度分级微纳米孔结构。在初始阶段，阳极氧化或微放电使纳米孔在表面形成。随着时间推移，微孔成核，由于四硼酸盐电解液可以溶解喷出的氧化物，从而避免氧化物沉积在微孔中。同时，具有较差绝缘性的深纳米孔存在于新形成的微孔附近，在微孔内等离子体放电的热效应下，该位置的绝缘性变得更低，导致下一个大的火花放电优先发生在该位置。因微孔每次仅向特定方向演化，导致形成“蠕形槽状”结构，各个“蠕形槽状”结构相互连通，从而形成“cortex-like”分级微纳米孔结构。

由此可见，微纳米孔形成原理主要集中在等离子体放电、放电微通道的形成、气体的释放、氧化物的熔凝效应以及电解液成分对涂层选择性溶解作用等。通过先进的表征手段，对火花放电行为及涂层组织结构（包括微纳米孔结构）的演化进行深入揭示，将为功能化涂层（成分/结构/表界面）设计与制备提供参考依据。

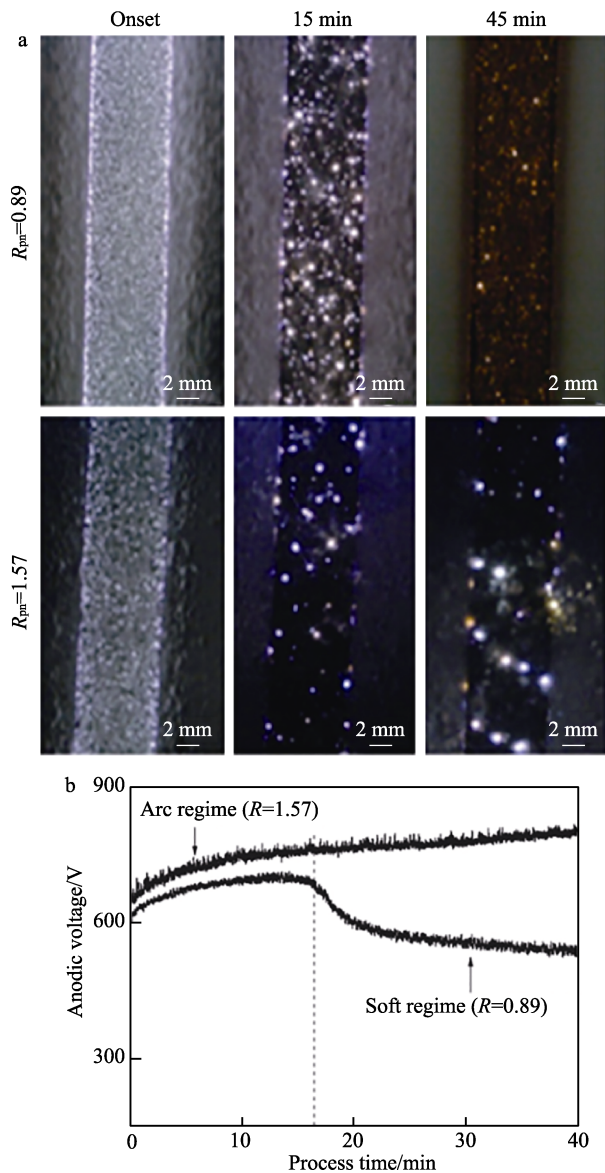
图 5 微弧氧化过程中的“软火花”放电模式^[41-42]

Fig.5 (a) The evaluation of plasma discharges as a function of the coating time obtained at $R_{pn} = 0.89$ and $R_{pn} = 1.57$ ^[41], and (b) Anodic voltage-time curves for 2214 Al alloy samples treated via MAO with $R_{pn} = 0.89$ and 1.57 where a soft sparking regime was observed after 15 min when the MAO process was carried out using a bipolar current mode with $R_{pn} = 0.89$ ^[42]

1.2 微纳米孔的存在形式与分类

通常，微弧氧化涂层结构可分为 2 层（阳极界面

层和外层），也可分为 3 层（阳极界面层、中间层和外层疏松层）^[45-46]，这与基体材料、电参数、电解液成分和处理时间密切相关。其中阳极界面层也称为过渡层，是基体与微弧氧化涂层之间的微区冶金结合界面；中间层为少缺陷、少气孔层，连接界面层和外层；外层是疏松多孔层。阳极界面层在阳极氧化阶段优先形成，但该层结构在氧化初期疏松多孔。随后，在阳极层中的垂直孔和球形孔内（孔尺寸小）产生持续的微弧放电，促进外层疏松多孔层的生长。随氧化时间增加，阳极界面层的孔中产生的精细放电和熔融冷却填充效应使致密的新阳极界面层形成。同时，孔内的电解液温度升高，对基底的刻蚀和氧化变得更明显，使涂层与金属之间形成波纹状界面，并在界面处形成水平孔（孔尺寸相对较大）^[47]。进一步，在涂层微纳孔内形成大量等离子体放电，该作用下中间层在阳极界面层的基础上开始生长，增加阳极界面层的致密性，并促进涂层生长。不同层结构对应微纳孔的分布形式分为：阳极界面孔、中间孔和表面孔。根据孔形貌分为：水平孔、垂直孔、球形孔以及弯曲孔等^[47]。涂层表面孔结构则更多样。

表 1 总结了微弧氧化涂层微纳孔的存在形式、分类及结构特点：

1) 阳极界面孔虽然存在，但数量较少。在精细放电过程中，产生的细微放电通道会使涂层形成阳极界面孔，但由于放电细小致密，且在熔融冷却过程中能瞬间填充孔洞，导致涂层界面孔很少，且尺寸较小，孔径一般在 100 nm 之内，平均孔径为 30 nm（大部分阳极界面孔尺寸在 50 nm 之内），孔隙率小于 1%。

2) 中间层内孔数量增加，但相比表面孔少很多。中间孔的产生在微弧氧化放电过程中是必不可少的，相对于表面孔，其孔尺寸小，且所形成的微孔一部分为连接涂层表面与界面层的连通孔，另一部分为盲孔。这是由于在微通道内的火花放电过程中，熔融物内层和外层的冷却速度不同，且熔融产物是在高温高压的作用下喷射出去，容易形成类似“倒三角”的连通孔洞。中间层内孔径一般在 100~600 nm，平均孔径为 300 nm，孔隙率小于 10%。

3) 表面孔形貌各异。在放电微区瞬间高温烧结形成熔融物过程中，等离子体反复击穿放电，使熔融氧化物聚集，并向外喷射。快速冷却后，使涂层表面

表 1 微弧氧化涂层微纳孔的存在形式、分类及结构特点

Tab.1 The existence form, classification and structural characteristics of micro-nano pores formed in MAO coatings

| Coating structure | Classification of pores | Micro-nanopore structure morphology | Size range | Average pore size | Porosity | Ref |
|-----------------------|---------------------------|--------------------------------------------------------------------------------------------------------------|------------|-------------------|----------|------------|
| Anode interface layer | Anode interface pores | Horizontal pore, vertical pore, section spherical pore and curved pore, blind pore, interconnecting pore etc | <100 nm | ≈30 nm | <1% | |
| Interlayer | Pores of the middle layer | | 100~600 nm | ≈300 nm | <10% | [19,36-54] |
| Outer layer | Surface pores | Various pore structures on the coating surface | 5 nm~10 μm | 1~5 μm | 5%~40% | |

形成不同形貌的大的孔洞，从而形成具有疏松多孔结构的外层。外层疏松多孔层形成的另一个原因可能是，孔洞内充满气体，气体由内向外释放的过程中，孔洞提供一个低阻力路径，但越向外部扩散，越容易产生大的阻力，导致气体逃逸时，出现“爆炸式”的释放，使得涂层表面孔洞较大。表面孔径一般为5 nm~10 μm之间，平均孔径为1~5 μm，孔隙率为5%~40%。

1.3 微纳米孔的定性或定量表征

通过先进的原位分析等手段表征微纳米孔结构，有助于深入分析多级微纳米孔结构形成过程与涂层生长机理，为涂层结构设计、功能调控提供参考依据。表2总结了微纳米孔先进的表征手段，并定性和定量地对孔结构进行系统性分析。

表2 微弧氧化涂层微纳米孔的先进表征手段

Tab.2 Advanced characterization methods of micro-nano pores in MAO coatings

| Summary of characterization methods | Special advanced characterization methods | Characterization analysis content | Micro-nano pore structure characteristics | Ref |
|----------------------------------------------------------------------------------------------------------------------------------------------------------------------------------|------------------------------------------------------------------------|--------------------------------------------------------------------------------------------------------------|-------------------------------------------------------------------------------------------------------------------------------------------------------------------------------------------------------------------------------------------------------------|---------|
| | Small area electrical monitoring system combined with X-ray tomography | Pore content, depth and morphology | The central hole extends to the whole coating, and even extends down to the substrate for a few microns. The hole near the substrate is 10 μm, and the surface pore is up to 100 μm. (porosity of 15%~20%) | [48] |
| | High resolution X-ray computed tomography (X-ray CT) | The location, size, and appearance of the holes | The porosity is about 5.7% and the coating thickness varies from 4 to 42 μm | [49] |
| | Synchrotron radiation tomography | 3D structure and 3D porosity | The initial stage shows a high porosity (up to 26.25%); The porosity decreases with the thickening of the oxide layer (from 26.25% to 10.88%) | [50] |
| TEM, FIB, SEM, In situ tensile, Synchrotron radiation, Tomographic slicing, Chemical stripping/Metallographic method, X-ray CT, GDOES depth profile, High-speed photography, OES | High speed video | Spark discharge information image: including discharge life, latency behavior, discharge characteristics | Individual discharges tend to occur in sequences (cascades), with lifetimes from a few microseconds to several tens of microseconds; Discharge lifetimes, and incubation periods, tend to increase as the thickness is raised | [51] |
| Nikon D300 digital camera | | Discharging behaviors; Coating growth kinetics; Cell potential-time responses | Pores are present in the inner part of the coating. A dense inner layer, ~1.2 μm thick, and a thicker outer layer, with through cracks, are evident. | [52] |
| | Optical emission spectroscopy, OES | The plasma electron temperature, electron density and atomic ionization in the plasma region were evaluated | The electron temperature in plasma discharge zone is about 3000~15 000 K; The initial spark density is high, then the spark becomes weak and less. In the later stage, the dense layer grows rapidly, while the loose outer layer thickness remains stable. | [53] |
| | Denudation coating combined with SEM and TEM | The “overgrowth” characteristics; The formation mechanism of micro/nano pores and crack propagation behavior | An interface layer (600 nm) composed of nanocrystalline and amorphous alumina | [45,54] |

T. W. Clyne 等^[19]从孔含量、孔结构和孔尺寸等方面进行了系统的研究，总结了微纳米孔的表征手段，如高分辨率扫描电子显微镜、静水压法、压汞法、氮比重瓶法、等温氮气吸附法（BET）等，孔隙率的测定方法包括理论孔隙率、表面孔隙率、体积孔隙率（骨密度）等。研究证实，在铝合金微弧氧化涂层表面存在表面连通的亚微米孔结构，孔的尺寸范围为5 nm~1 μm，平均直径约30 nm，孔隙率约20%，体密度约为3 g/cm³。此外，S. C. Troughton 等^[48]还开发了微区电气监控系统（Gordon Laboratory in Cambridge），可

拍摄相当高分辨的SEM显微照片，并结合X射线断层成像技术，揭示等离子体放电产生的局部级联反应对涂层孔结构演变的影响，特别是对孔含量、孔深度和孔形貌等的演变产生的重要作用。由涂层中级部位微纳米孔的典型结构（如图6所示）可看出，放电位置（红色虚线）是涂层微观结构外观发生实质性变化的唯一位置。当重复操作时（样品再次置于电解液中，处理1 s），级联反应在同一位置继续进行，这证实了在同一位置促进重复放电的是局部孔结构。同时，深孔的存在稳定了持续放电的位置，形成了一个

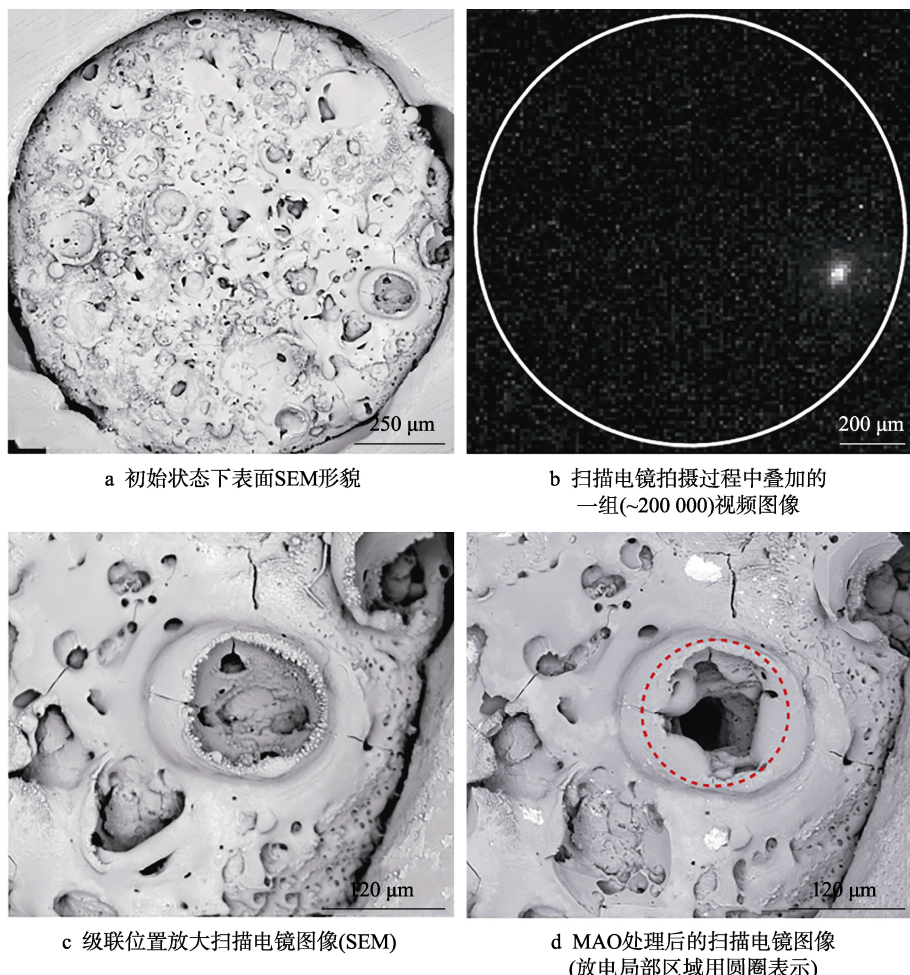
图 6 放电级联在 2500 Hz 下持续 1 s 对涂层微观结构的影响^[48]

Fig.6 Microstructural effects of a discharge cascade on a small area sample (with 100 μm MAO coating) at 2500 Hz for 1 s: a) SEM of the surface in the initial state; b) superimposed set of ($\sim 200\,000$) video images taken during the process; c) magnified SEM of the region indicated in (b) as the cascade location; d) the same area after MAO processing (with the region in which the discharges were localised indicated by circles)^[48]

相对较低的电阻区域，从而进一步形成较大且深的孔洞^[48]。以上述操作处理样品，其放电通道形成的 3D 孔结构极不规则，中心孔几乎延伸到整个涂层，甚至向下延伸至基体几微米，且基体仅被 1 μm 或几微米薄的氧化物层所覆盖（如图 7 所示）。孔尺寸随深度的增加而逐渐减小，其中基体附近的孔直径为几十微米，而表面火山口位置的孔直径可达 100 μm ，且涂层中孔洞相互连通（见图 7d—g）。然而，尽管微弧氧化涂层是多孔的（孔隙率约为 5%~40%），但它们通常不包含该文献中所提到的如此大的孔洞。这是由于随着氧化时间的延长，孔附近会产生新的微弧放电，大的孔洞在熔融冷却过程中能瞬间被填充^[34,48]。

P. Skeldon 等^[49]利用高分辨率 X 射线计算机断层成像技术，定性研究了微弧氧化涂层孔洞的位置、大小和形貌，测得孔隙率为 5.7%（如图 8 所示），涂层厚度为 4~42 μm ，较厚的涂层区域与涂层表面上的结节、大孔和氧化层增加有关。揭示了结节下面孔的连通性，能鉴定直接向涂层表面开放的通孔和终止于涂层表面的盲孔，更直观地证明了孔洞是由熔融涂层

中的放电通道内释放出的氧气产生的。Lu X. P. 等^[50]利用同步辐射显微层析成像技术，研究镁合金微弧氧化涂层的相组成和相变的内部结构，包括三维组织结构和三维孔隙率，为揭示和理解涂层孔隙率的性质，对其大小、体积、演化和分布特征进行了定性和定量研究（如图 9 所示）。微弧氧化涂层的初期阶段表现出高孔隙率（高达 26.25%），涂层的孔隙率随着氧化层的增厚而降低（从 26.25% 降到 10.88%）。同时发现，涂层表面的多孔性可能是由一个大的孔或者缺陷引起的，并证明微弧氧化涂层的外层和内阻挡层之间存在孔隙带。利用层析切片法发现，整个涂层都存在不同尺寸的微纳米孔缺陷，而用传统金相镶嵌制取涂层截面，进行扫描观察，几乎看不到缺陷，这是由于涂层截面在抛光过程中，产生涂层碎片，被嵌入并保留在孔洞和缺陷中^[50]。A. Nominé 等^[51]对铝微弧氧化涂层的生长过程进行了高速摄影成像，捕获了涂层生长微秒级别的火花放电信息图像，通过放电寿命、潜伏期行为、放电特性等，揭示了微弧氧化过程中发生在微区的瞬间反应，对涂层微纳米孔的形成原因和生长

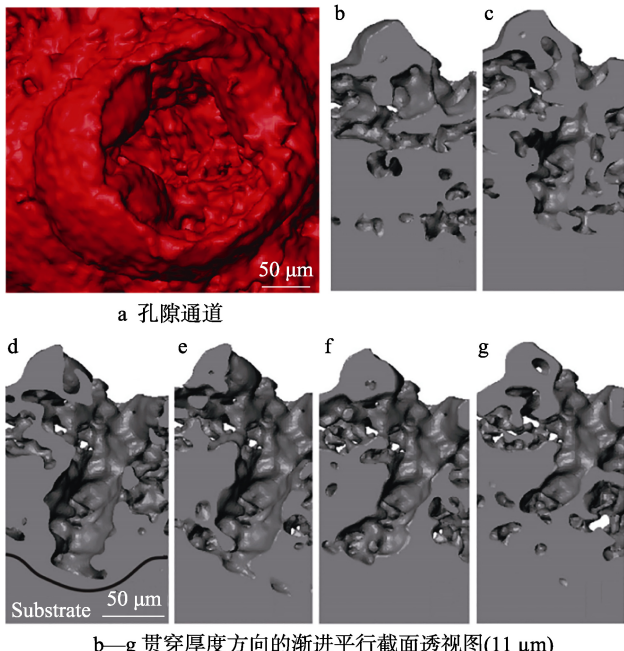


图7 级联部位的微纳米孔的典型结构^[48]

Fig.7 Tomographic data from the circled region of the small area sample in Fig.6d: a) a perspective view into the pore channel and (b—g) progressive parallel sections (11 μm apart), containing the through-thickness direction, with sections (d) and (e) located near to the approximate axis of the pore^[48]

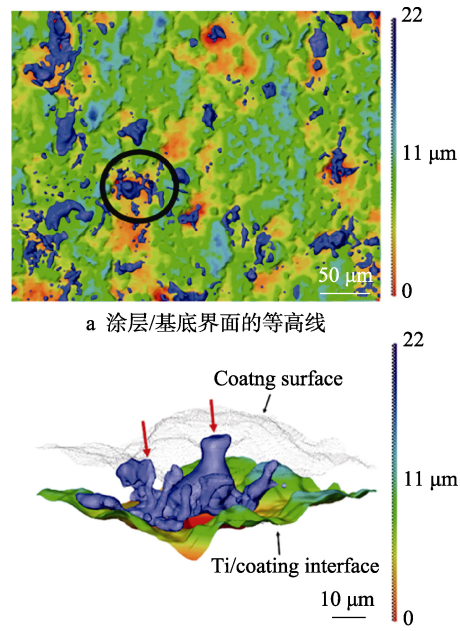


图8 高分辨率X射线计算机断层成像^[49]

Fig.8 High resolution X-ray computed tomography (X-ray CT): a) contour plot showing the coating/substrate interface, the color scale shows the height of the coating/substrate interface, measured in microns with respect to the lowest point of the interface, pores have been rendered (in blue) showing their spatial correlation with respect to interface undulations; b) a zoom-inside view is shown for the volcano-like pore^[49]

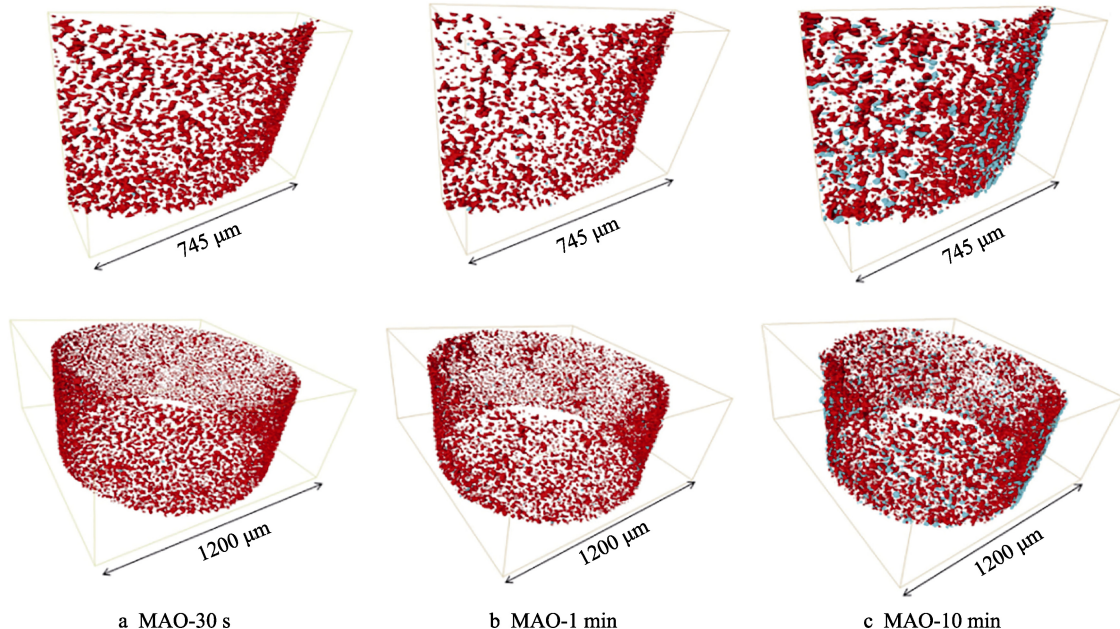


图9 涂层中孔（红色）和颗粒（浅蓝色）的分布（同步辐射显微层析成像）^[50]

Fig.9 Distribution of the pores (in red) and particles (in light blue) in the coatings^[50]

行为提供了进一步的证据。Cheng Y. L.等^[52]利用尼康D300数码相机记录了火花放电行为,建立了放电模型,以揭示涂层生长动力学和微纳米孔结构形成方式。Xue W. B.等^[53]通过分析光发射谱(OES)的谱线,评估了等离子体区中的等离子体电子温度、电子密度和

原子电离度,并发现等离子体温度曲线上高尖峰的出现取决于火花密度和光照强度,而不是大的放电火花,特别在微弧氧化后期,涂层的中间层快速生长,而外层疏松层厚度保持稳定。Wang Y. M.等^[54]利用剥蚀微弧氧化涂层,再结合扫描电镜,表征等离子放电

在基材/涂层界面上引起的局部“过生长”特性，并利用透射电镜发现，基体/涂层界面处形成由纳米晶体和非晶态 Al_2O_3 组成的薄粘结层，即约 600 nm 厚的致密界面层（如图 10 所示），利用原位拉伸揭示了涂层“过生长”区域附近的微纳米孔形成机制和裂纹扩展行为^[45]。上述先进的微纳米孔表征方法可以有效

地定性和定量分析涂层中孔含量、孔大小、孔结构、孔分布和数量，以及微纳米孔之间相互联系的自然形态特征，弥补常规电子显微镜和分析方法的研究缺陷，更直观地理解分析涂层微纳米孔结构的生长模型机制，为涂层结构设计、特种功能实现奠定理论依据。

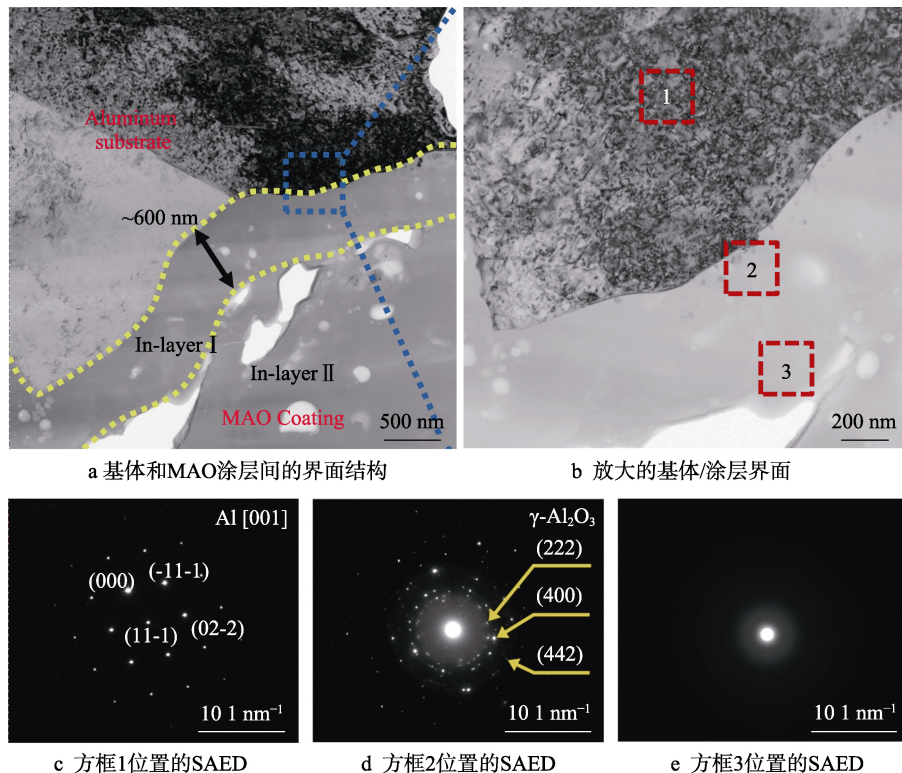


图 10 600 V 氧化 30 min 时 MAO 涂层的 TEM 图像^[54]

Fig. 10 TEM image of MAO coatings under 600V with oxidation time of 30 min: a) a distinct interfacial structure between substrate and MAO coating; b) Magnification of substrate/coating interface from a (as the blue square shown); c) Selected area electron diffractions (SAED) of red square 1 inserted in (b); d) SAED of near substrate/coating interface red square 2 inserted in (b); e) SAED of MAO coating (red square 3 inserted in (b))^[54]

2 涂层微纳米孔结构形成的影响因素

在探究涂层中微纳米孔结构及形成影响因素的基础上，通过制备工艺参数来调控多级微纳米孔结构的定制化形成、减少（甚至消除），将为构建特殊功能的涂层结构及体系提供途径。影响涂层微纳米孔结构形成的因素包括：基体材料、电解液成分、pH、电解液温度、电导率、电源模式、电参数等。其中，电解液成分、电源模式和电参数对微纳米孔结构的控制起着决定性作用。为了满足特种服役环境的使用要求，需要采用预处理、后处理、特殊电解液、电源模式以及电参数来匹配调控涂层的微纳米孔结构。

2.1 电解液

2.1.1 组分

A. V. Timoshenko 等^[55]发现，在碱性电解液中，阳极反应生成的金属离子及其他金属离子易于转变成

带负电的胶体粒子而重新进入涂层，并通过调整和改善涂层中微纳米孔结构而获得新的特性，因而电解液体系由早期的酸性发展为现在的碱性，并被广泛应用。碱性电解液体系多由吸附能力较强的阴离子对应的溶液构成。阳极氧化膜对溶液中阴离子的选择性吸附研究结果表明^[56-57]，阴离子吸附能力由强到弱排列次序为： $\text{SiO}_3^{2-} > \text{PO}_4^{3-} > \text{VO}_4^3 > \text{MoO}_4^3 > \text{WO}_4^3 > \text{B}_4\text{O}_7^2 > \text{CrO}_4^3$ 。硅酸盐和磷酸盐成为碱性电解液的两大主要体系，此外铝酸盐体系、碱金属的氢氧化物体系也是选择的对象。另外，从涂层物相成分、组织结构的角度，将电解液的作用分成以下几类^[58-59]：1) 仅提供氧进入涂层的电解液；2) 电解液中包含有阴离子组分，可提供其他元素进入涂层；3) 电解液中包含有阳离子组分，可提供其他元素进入涂层；4) 提供对宏观粒子进行阴离子传输的悬浊液，这种宏观粒子有助于涂层形成；5) 不同电解液成分对涂层具有选择性溶解作用，提高涂层孔隙率，形成分级微纳米孔结构。

表3总结了典型电解液对微弧氧化涂层微纳米孔结构的影响。可以看出,硅酸钠的添加^[60-61],使溶液电导率增大,起弧电压降低,易于形成钝化膜。同时 SiO_3^{2-} 与电解液中的其他阴离子协同作用,使得阳极表面微观电位强弱区的对比态势加剧,促使放电火花的燃、熄两种状态在基材表面此起彼伏,交替进行,加速了放电火花在基材表面的游移,从而避免局部热量累积有可能导致的宏观小凹坑出现,以及微裂纹的产生,可同时提高涂层厚度和整体致密性。添加磷酸盐^[62-63]可以增加涂层厚度,降低表面粗糙度,使涂层更加平滑致密,且微孔数量明显减少。铝酸钠及其氢氧化物的添加^[64-67]会使电解液电导率大幅度提高,降低起弧电压,调节电弧大小,从而促进涂层厚度均匀增加,避免产生大的孔洞,并减少微裂纹。四硼酸盐的添加^[44,68-69]会使在微弧放电过程中形成的氧化物溶解在电解液中,很少或没有沉积在放电通道外,可构建出双尺度“cortex-like”状复合结构,导致涂层表面形成具有相互连通的分级微米孔和纳米孔结构。添加 Na_2WO_4 、 Na_2SnO_3 、 Na_2MnO_4 等^[70],可以同时

增加涂层厚度和表面粗糙度;在电解液中加入甘油等,可以稳定微弧放电火花,使涂层孔隙率下降;添加氢氧化钾或氢氧化钠等,可以调节电解液的pH值;添加 $\text{Na}_3\text{C}_6\text{H}_5\text{O}_7 \cdot 2\text{H}_2\text{O}$,可提高电解液稳定性、电导率,从而提高涂层的生长速率和厚度,有助于耐蚀性的提高^[71]。其中,pH值越大或电导率越大,会降低起弧电压,有利于涂层致密层的快速形成,从而提高涂层的厚度、致密度,并防止外层疏松层产生大的孔洞;但pH或电导率过大,会使涂层孔隙率增大,表面更加粗糙,降低涂层致密性,使表面质量下降。另外,F. Simchen等^[72]研究了电解液电导率对起弧电压的影响,结果表明,决定起弧电压的不是电解液电导率,而是电解液/基体界面上的电子注入能力。这种注入能力取决于电解液中阴离子的种类和浓度。A. B. Rogov等^[73]研究了交流极化条件下,阳离子电解液的组成(Li^+ 、 Na^+ 、 K^+)对铝合金微弧氧化过程电学和光学响应的影响。研究发现,在钠离子和钾离子存在下,微弧氧化的阳极电流-电压曲线具有明显的滞后性(出现“软火花”特性)。

表3 典型电解液对微弧氧化涂层微纳米孔的影响

Tab.3 Effect of representative electrolyte on micro-nano pores formed in MAO coatings

| Electrolyte | Film-forming rate | Coating structure | Porosity | Ref |
|------------------------------|----------------------------------------|-------------------------------------------------------------------------------------------------------------------------------------------------------------|----------------------------------------------------------|---------------|
| Na_2SiO_3 | Fast | Thick coating; High density; High porosity; Less cracks | Dense inner layer and porous outer layer | |
| Phosphate | Moderate | Thin and dense coating; Small roughness; Surface smoothing; Less cracks | Low porosity and thin inner dense layer; Small pore size | |
| NaAlO_2 , hydroxide | Fast | Thick and dense coating; High density; Less cracks | Low porosity; Dense inner layer | [24,36,55-73] |
| Tetraborate | Moderate; Strong selective dissolution | Morphology of cortex-like slots; High porosity; Micro/nano Hierarchical micro-nano structures; Dual-scale structure that contained microslots and nanopores | Micro/nano hole; Uneven coating thickness | |

2.1.2 浓度

电解液浓度增加,可提高微弧氧化反应的生长速率和程度,在此基础上,调节电解液不同成分的比例,可大幅度调控微纳米孔的尺寸、分布和数量,并不同程度地提高涂层厚度,优化涂层的表面特性。电解液浓度降低,有利于防止涂层中孔隙的产生,也有利于减小孔径尺寸。但是,电解液浓度太小(反应难以进行,不利于成膜)或太大(反应太剧烈,不利于形成致密膜,甚至对涂层产生腐蚀作用),都不利于涂层的生长和微纳米孔结构的调控,从而阻碍表面功能化改性。

2.1.3 特殊微纳米粒子

将特殊离子、分子、微纳米金属/陶瓷/聚合物粒子等添加到电解液中,对涂层的微纳米孔结构和性能会产生很大的影响。将其引入到涂层内,可以调控涂

层表面特殊微纳结构。例如,将陶瓷纳米粒子作为添加剂添加到电解液中,大量的添加粒子会在涂层中大的孔洞和缺陷附近处优先聚集,并烧结沉积生长。大部分粒子主要位于涂层的外层和中间层,说明添加的粒子通过放电通道可以随熔融的陶瓷层氧化物回流,并随着陶瓷层一起生长,在孔洞周围团聚^[50]。同时,大量粒子聚集形成大尺寸颗粒或多层结构复合涂层,从而调控不同结构的微纳米孔,实现功能特性,以满足不同环境服役的需求^[74-76]。有机纳米粒子添加到电解液中,会和陶瓷层同时生长,在孔洞内聚集,并实现密封,有利于提高涂层的耐蚀性、电绝缘性,以及构建特殊微纳米表面结构,并结合低表面能,实现疏水性,满足功能化应用要求^[77]。

由此可见,针对电解液而言,涂层生长的前提条件是介质击穿。为了优化涂层生长,控制涂层孔结构,可以利用提高金属强钝化的添加剂以降低起弧电压,

促进金属/涂层/电解液之间的界面反应, 从而控制涂层孔隙率, 提高涂层致密性, 加快涂层生长。通过调控电解液配方, 综合考虑单一电解液成分对涂层生长的影响, 将 2 种或 2 种以上的电解液成分混合搭配使用, 能更好地稳定涂层微弧放电, 从而达到同时提高涂层厚度和致密度的目的。

2.2 电源模式和电参数

电源及其输出控制模式确定了微弧氧化过程中电压输出方式, 进而决定了作用于单个微弧放电的能量分布与持续时间。该过程显著影响氧化物生成速率与涂层表面、界面的结构特性。

直流电源可制备大厚度的微弧氧化涂层($100\text{ }\mu\text{m}$ 以上, 甚至更厚), 但涂层表面及中间微孔尺寸大、数量多, 且耗能高, 不利于节能环保。与直流电源相比, 当使用交流电源时, 该工艺运行更有效, 涂层质量更高^[78-81]。双极电流模式, 可对涂层中间与表面的微纳米孔进行调控, 制备的涂层质量更高, 且节能环保。特别地, 在双极脉冲电源模式下, 利用负脉冲在“软火花”或“烧结电弧”等新型火花放电模式辅助下, 通过向涂层引入更多电解液中的物质和改进的放电火花类型, 可促进均匀致密涂层的形成^[82-84]。

单位脉冲放电能量决定了涂层的生长效率、物相成分以及微纳米孔的形态演变。一般而言, 频率越高或占空比越小, 单位脉冲放电能量越低, 则涂层表面和内部的微纳米孔越小, 粗糙度越低, 厚度也越低, 并且会减少连通孔和长裂纹, 孔隙率下降。单位脉冲放电能量增加, 使每次击穿过程中产生熔融氧化物的量增大, 有利于涂层快速生长, 但放电通道冷却凝固后, 留下的微纳米孔的孔径增加, 易形成疏松多孔的外层(粗糙度增加, 致密度下降)。控制微弧氧化过程中不同氧化阶段的能量分布策略, 可改善涂层致密性^[85]: 在微弧氧化初期, 利用强脉冲放电作用, 使得涂层厚度迅速增加, 并促进内层致密层的形成; 后期, 通过降低电流密度以及调节频率和占空比, 使单位脉冲放电能量减小, 在相对较弱的放电强度下进行微弧放电, 微弧放电击穿只发生在涂层相对较薄弱或有缺陷的位置, 如此重复击穿, 可对前期形成的疏松多孔层(含缺陷)进行一定程度的愈合和修复, 从而提高涂层致密性。

2.3 其他因素

除了以上主要影响因素外, 其他因素(基体材料、电解液温度等)对涂层微纳米孔结构的形成也有影响。其中, 对于不同的原材料而言, 由于其所含元素不同, 呈现出不同的成膜特性。电解液温度越高, 形成的涂层越厚, 且孔的尺寸变大, 孔隙率增加, 表面也越粗糙, 使得涂层质量下降。

3 涂层微纳米孔结构形成的控制策略

由以上讨论可知, 陶瓷涂层的生长速率、致密性以及微纳米孔结构, 可以通过电解液和电参数进行优化设计。针对不同服役环境对涂层微纳米孔结构及特殊功能性的需求, 总结了涂层纳米孔结构调控方法和策略, 见表 4。

3.1 构建孔

特殊功能应用的场合, 需要特定尺寸的微纳米孔, 以调控与优化涂层的性能。如热控涂层与入射光谱的匹配孔尺寸在纳米级到几十微米; 生物涂层与骨组织长入匹配的孔尺寸在微米级(几微米~ $200\text{ }\mu\text{m}$); 锂电池、超级电容器以及染料敏化太阳能电池电极活性涂层为获得更高的存储容量, 就要更大的比表面积, 因此需要涂层中间孔与表面孔在三维空间贯通匹配。但受微弧氧化涂层中孔尺寸控制难等因素制约, 如何按需构建具有特定分布与尺寸的微纳米孔, 是巨大挑战。构建大尺寸孔: 电源模式可采用直流或单极脉冲; 适当提高脉冲电压、电流密度以及增加氧化时间; 提高电解液电导率, 掺杂特定改性物质; 多步复合扩孔(酸化、氟化、腐蚀)等。构建小尺寸孔: 电源模式可采用双极脉冲(非对称式); 适当降低脉冲电压、电流密度以及减少氧化时间; 调节电解液电导率, 掺杂特定改性物质; 多步复合缩孔(掺杂、填充)、外场辅助等。构建多级微纳米孔: 采用多步升压工艺方式; 调节电解液电导率和掺杂特定添加物; 多步骤扩孔+缩孔(化学、电化学、热处理)或外场辅助等来形成多级微纳米孔结构。

Yao Z. P. 等^[86]综述了微弧氧化技术在热控涂层中的应用, 提到增加氧化时间和提高电流密度, 使涂层厚度增加, 粗糙度变大。在电解液中添加阴、阳离子或纳米/微米颗粒, 调控不同组分和表面微纳米孔结构在涂层中的分布, 从 $1\text{ }\mu\text{m}$ 到几十微米不等, 其中小孔隙有助于提高太阳吸收率, 大孔隙则有助于提高发射率。H. Hornberger 等^[87]综述了可降解镁及镁合金表面微弧氧化涂层在生物医学领域的研究进展, 确定并讨论了决定涂层性能的关键因素(如涂层形貌、附着力、孔隙率、腐蚀速率和表面化学性质), 并提出了涂层微纳米孔结构对于调控可降解镁合金降解速率的要求, 即内层致密, 外层多孔(孔径约几微米到几十微米)。M. Geetha 等^[88]综述了钛基生物涂层力学、生物相容性、耐磨性以及耐腐蚀性等与微观组织结构的关系, 并从构建微纳米孔结构尺寸分布、提高表面孔隙率、增加表面粗糙度、添加生物活性成分等方面, 提高钛及其合金的耐磨性和骨整合性, 从而提高植入手的功能寿命。Wei D. Q. 等^[12,89]通过化学、热处理及水热处理等技术对微弧氧化涂层进行复合改性, 获得合适孔径的多级微纳米孔结构, 可有效

表 4 微弧氧化涂层微纳米孔结构的控制策略、性能及应用
Tab.4 The tailoring strategy, properties and applications of micro-nanopores formed in MAO coatings

| The tailoring of micro-nanopores | Electrolyte systems | Electric parameters | | | Micro-nanopore structure | Properties | Application | Ref |
|----------------------------------|----------------------------------------------------------------------------------------------------------|------------------------|-------|----------|--------------------------|-------------------------------------------------------------------------------------|-------------------------------------------------------------------------|--------------------------------------------------------|
| | | Voltage/current | t/min | f/Hz | D/% | | | |
| Construct pore | Na ₂ SiO ₃ +Na ₃ PO ₄ +NaAlO ₂ | 550 V | 60 | 600 | 8 | Size range: 1~20 μm Average size: 5 μm ($R_a=2.5$) | Emissivity 0.85 (700 °C) | Thermal radiation [108] |
| | C ₃ H ₇ Na ₂ O ₆ P, Ca(OH) ₂ ⁺ NaOH+HT | 450 V | 10 | 100 | 26 | Narrow interrod HA nanorods | i_{corr} : Decreases 3 orders of magnitude, high bonding integrity | Anti-corrosion, Mechanical, Cytocompatibility [109] |
| | Na ₂ SiO ₃ +KOH+KF+LDHs | 0.3 A/cm ² | | 800 | 10 | Double-layer, nanosheet | i_{corr} : Decreases 2 orders of magnitude, | Anti-corrosion, Cytocompatibility, Drug delivery [110] |
| | Na ₂ SiO ₃ | 0.1 A/cm ² | 10 | | | “Sheet” (Co ₃ O ₄), “grain” (CuO) and “hedgehog” | Activation energy $E_a=42.6\sim141.8$ kJ/mol | Photocatalysis [111] |
| Eliminate pore | H ₂ SO ₄ ⁺ Na ₂ SiO ₃ +SiO ₂ | 200 V | 5 | | | Size range: 0.05~0.2 μm (no SiO ₂), 0.8~1.2 μm (with SiO ₂) | High capacity, cycling stability | Lithium-ion battery anodes [14] |
| | NaOH+Na ₂ SiO ₃ +Na ₃ PO ₄ | 20 mA/cm ² | 10 | 200~1000 | | Pore diameters: 0.5~1 μm Porosity: 7%~14% | Bonding strength, EIS results | Anti-corrosion, Mechanical [92] |
| | NaOH+phytic acid+polymethyltrimethoxysilane | 220~250 V | 10 | 100 | 50 | PMTMS sealing pores, clusters of spherical particles | i_{corr} : decreases 3 orders of magnitude, Self-healing | Anti-corrosion [112] |
| Prefabrication pore | NaAlO ₂ +Na ₂ SiO ₃ +(NaPO ₃) ₆ | 550 V | 20 | 500~700 | 8~10 | Porous, island-like morphology, large irregular particles | 800 °C for 150 h, 53.44% and 24.97% of the bared Ti ₂ AlNb | Oxidation resistance [94] |
| | Na ₂ SiO ₃ +KOH+(LDHs) | 1 A | 20 | | | Nanoplatelets grow on the pores with inhibitors | Healing effects, EIS, long-term immersion stability | Anti-corrosion [113] |
| | Na ₃ PO ₄ +Tb ₄ O ₇ particles | 150 mA/cm ² | 10 | | | Porous structure of different sizes | Improve photocatalytic activity | Photocatalysis [114] |
| | Na ₃ PO ₄ | 325 V | 5 | 3000 | | Different microstructures, Co- corrosion morphology | 28-days immersion stability, corrosion product layer inhibits corrosion | Anti-corrosion [103] |

调控表面细胞与组织的附着行为。Liu B. D.等^[90]利用微弧氧化法将具有不同 Co 浓度和可调尺寸的非贵金属(Ni_{1-x}Co_x)₅TiO₇ 纳米结构原位整合到柔性金属网络载体上，不同 Co/Ni 比直接导致涂层不同的尺寸和形态演变，从而确定 x=0.16 的(Ni_{1-x}Co_x)₅TiO₇ 纳米线阵列具有对 CO 催化氧化的最佳性能以及良好的催化稳定性。G. Lee 等^[14]利用微弧氧化制备 SiO₂/TiO₂ 复合膜作为电池的负极，随二氧化硅含量的增加，微弧氧化膜层中的微纳米孔尺寸、含量发生变化，并且通过调节多级微纳米孔结构和物相成分，为 Li⁺的扩散提

供了路径和通道，使该涂层具有优异的电池容量和循环稳定性。

3.2 消减孔

一些应用场合需要消除微纳米孔，或降低孔隙率。如金属长期腐蚀保护、耐磨减摩、热防护、介电绝缘等。可采取的策略如下：通过调节电源模式，使放电火花均匀致密(如采用双极脉冲、提供阴极放电、“软火花”放电等)；调控电解液成分，掺杂特定改性物质，构建自封闭或自愈合的物相结构；控制电参

数, 采用多步骤升压方式, 初期高电流密度形成致密性高的内层, 后期低电流密度对多孔层的孔隙和缺陷进行弥补和愈合; 多步复合处理(超声辅助、水热、水汽、碱热、旋涂、浸涂等)进行封孔, 提高涂层的致密性。

Cui C. X. 等^[91]通过调节不同氧化时间, 调控其孔形貌和尺寸大小, 降低孔隙率, 以提高涂层整体致密性和耐蚀性。Zuo Y. 等^[92]采用高频双极脉冲模式制备 AZ91D 镁合金微弧氧化膜, 研究了孔隙率和孔参数对涂层性能的影响。随电流频率的增加, 孔洞直径和孔隙率减小, 介孔间距和孔圆度增大。高的孔隙率可使涂层开裂, 而较大的介孔间距和高的孔隙圆度可阻碍涂层开裂; 低的孔隙率和裂纹密度, 有利于提高涂层的耐热性和抗腐蚀性。J. R. Smith 等^[93]综述了在航空航天器表面和结构上利用新型涂层和表面处理技术的最新进展, 提到低孔隙率有利于提高腐蚀和磨损防护。Ouyang J. H. 等^[94]利用微弧氧化技术制备了耐高温抗氧化涂层, 通过调节不同电解液成分, 制备的内层致密、外层多孔涂层使基体获得优异的耐高温稳定性。Shen D. J. 等^[95]通过调控电流密度和氧化时间, 降低了铝合金表面涂层的孔隙率, 提高了陶瓷涂层的电绝缘性。K. M. Lee 等^[96]通过在电解液中添加氟化物, 结果发现形成低熔点的 MgF₂ 分布在整个涂层上(不仅存在于涂层外层, 也存在于内层), 这对于镁合金微弧氧化涂层孔的自封闭是有利的。SONG Y. W. 等^[97]利用 K₂ZrF₆ 电解液在镁合金表面制备了 MgO 和 MgF₂ 复合陶瓷涂层, 涂层具有较好的封孔效应和耐蚀性。另外, 在微弧氧化电解液中添加微纳金属/陶瓷/聚合物粒子^[98], 也可以减小孔数量或使微纳孔密封, 有效降低孔隙率, 提高涂层综合性能。笔者提出微弧氧化-纳米粒子(金属/陶瓷/高分子颗粒)等离子辅助同步交联(烧结)高效构建大厚度多层复合涂层的新技术^[99-100]。该技术通过在电解液中添加有机/无机纳米粒子, 在等离子体诱导下, 纳米粒子发生活化, 使大量的纳米粒子沉积, 并同步烧结(交联沉积)形成大厚度纳米粒子的外层, 与微弧氧化底层形成多层复合涂层。该涂层可对孔进行有效地消除和封闭。

3.3 工艺孔

利用微弧氧化涂层表面独特的工艺孔结构, 进而控制微纳孔尺寸、形貌以及分布, 以匹配后处理改性技术增强或赋予新的功能特性, 越来越受到关注。V. S. Rudnev 等^[101]制备了多孔结构的微弧氧化涂层, 并添加催化性高的过渡金属氧化物, 优选出催化活性高的涂层。Wu L. 等^[102]利用微弧氧化多孔结构为底层, 制备了双氢氧化物多层复合涂层, 该涂层具有很好的自愈合能力, 可为镁合金基体提供长期有效的腐蚀保护。Gu Y. 等^[103]通过在微弧氧化工艺孔中添加和渗入缓蚀剂, 提高了涂层的耐蚀性能^[103]。还有研究

者利用微纳金属/陶瓷/聚合物粒子添加^[104]、封孔剂、溶胶凝胶法^[106]、聚合物复合法^[107]等制备以微弧氧化层为底层的多层结构复合涂层, 提高了基体的防护和功能性应用。

4 涂层微纳孔结构调控与功能性应用研究进展

4.1 抗磨减摩

轻质高强金属(如钛合金、铝合金、镁合金)作为相对运动部件, 可代替高强钢等材料, 在轻量化减重增效中起关键性作用(减重约 50%), 然而轻金属耐磨性差严重制约了其扩大应用。相比于化学转化与传统阳极氧化膜层, 微弧氧化涂层具有高膜基结合强度与高硬度等优点, 且通过调节电源模式、电参数、特定掺杂改性、多层结构复合等方式控制微纳孔的形成(表 5 中 5-1), 提高内外层致密性, 可获得厚度可控、孔隙率低(致密度高)、耐磨减摩密封性优异的涂层, 在轻质高强金属的耐磨、减摩、动密封方面具有应用潜力^[115-120]。

4.2 耐腐蚀

轻质高强金属构件服役于海洋环境中, 容易发生腐蚀, 甚至失效(海水腐蚀、盐雾腐蚀、环境温度腐蚀以及霉菌腐蚀等), 这严重限制了轻金属的使用范围和服役寿命, 微弧氧化涂层及其复合改性层可提供有效的防护。从微弧氧化电参数、电解液、粒子掺杂改性、复合处理等角度入手, 通过涂层结构的设计(表 5 中 5-2), 提高内层致密层厚度, 降低外层疏松层的孔隙率, 可有效提高涂层的抗腐蚀性^[121-122]。此外, 利用后处理工艺, 以多孔的微弧氧化层为打底层, 制备多层结构复合涂层, 也可提高涂层的抗腐蚀性^[123]。Wang Y. M. 等^[124]通过金属基体表面纳米化预处理, 改善了内层致密层的特性, 可同时提高涂层的抗疲劳与抗腐蚀。微弧氧化层表面固有的多级微纳孔结构, 为缓蚀剂的掺入和纳米粒子的填充提供了很好的模板。缓蚀剂被包裹在微弧氧化涂层的开孔中, 并利用溶胶-凝胶、涂料、聚合物等进行复合和封孔, 以制备高阻隔性的重防腐复合涂层^[125-127]。

4.3 热防护

轻质高强金属在高速飞行器中的用量日趋增加, 但低熔点金属在高速空气摩擦时容易变形失效, 需要抗氧化、低热导系数或高辐射散热涂层体系。通过调节微弧氧化电源模式和电解液成分、浓度(表 5 中 5-3), 可在金属表面调控出大厚度、高结合强度的隔热微弧氧化陶瓷涂层, 涂层内层致密, 外层疏松多孔, 具有低热导率隔热(<1 W/(m·K))、高抗热震性、优

表 5 金属表面功能性涂层微纳孔结构特点

Tab.5 Structural characteristics of micro-nano pores formed on metals for functional characteristics

| Serial number | Functional characteristics | Micro-nanopore structure characteristics | Properties | Application | Ref |
|---------------|----------------------------------|--------------------------------------------------------------------------------------------------------------------------------------------------------------------------------------------------------------------------------------------------------------------------------------------------------------------------------------------------------------------------------------------------------------------------|----------------------------------------------------------------------------------------------------------------------------------------------------------------------------------------------------------|---------------------------------------------|------------------|
| 5-1 | Wear resistance and antifriction | Thick, dense layer; low porosity; The inner layer has a uniformly distributed nanocrystalline; Hole sealing; Wear-resistant particle doping; Composite modification of low friction coefficient materials | Low coefficient of friction Nanoparticles can improve wear resistance High adhesive strength | Wear resistance and antifriction | [115-120] |
| 5-2 | Corrosion resistance | Thick, dense layer; Low surface porosity; low roughness; Pores are shallow and closed; Particle doping modification Hole sealing; Corrosion inhibitor; High inner layer density | High corrosion potential; Low corrosion current; High impedance modulus; Long-term chemical stability; | Corrosion resistance | [121-127] |
| 5-3 | Thermal protection | Porosity<10%; Networks of fine-scale porosity; Dense layer; Multi-layer structure; Sealing pores; Porous crater-like morphology; Multiscale pore; Bridged structure | Low thermal conductivity: 0.5 W/(m·K) Improving oxidation resistance Low parabolic rate constant | Thermal protection and oxidation resistance | [128-130] |
| 5-4 | Thermal control | High surface roughness; Flower-like structures, micro-papillae, randomly staggered nanoplatelets Multilayer structure; Surface with numerous nanoparticles, $R_a=3.41 \mu\text{m}$, Porosity≈1.87~12.72 Micro-porous with different shapes and sizes $R_a=0.5\sim0.8 \mu\text{m}$, porosity reduces from 7.5% to 1.8%, particles filling pores; Nano-clusters, Fractal structure; Porous structure with different size | Emissivity (>0.8) (3~20 μm) Solar absorptance: 0.439~0.918 Absorptance: 0.35 (200~2500 nm), Emissivity 0.8 (873 K) (0.25~2.5 μm) | Thermal radiation and Thermal control | [131-138] |
| 5-5 | Insulation and dielectric | Low porosity; compact inner layer; small cracks; Thick, smooth and compact coating | High resistance; High breakdown voltage; high dielectric strength; high electrical resistivity; Excellent dielectric property and ferroelectricity | Insulation, dielectric and ferroelectric | [66,97, 139-141] |
| 5-6 | Biomedical properties | Microscale pits; Petal-like nanostructures; Granular nanostructures; Microbead; Macroporous structure=300 μm , micropores of 2~5 μm ; Sr-HA Nanorods on Micropores; Nanogranulates, micro/nanoscaled hierarchical surfaces; Dense inner layer; Needle-like outer layer; Sealing effects; Cortex-like structure | Promote cell attachment and osteogenic differentiation; High interface bonding strength; Excellent osseointegration; Cytocompatibility and blood compatibility; Low corrosion current and corrosion rate | Biomedical and anti-corrosion, | [142-151] |
| 5-7 | Catalysis | V-doped TiO ₂ nanosheets; FeO _x , SiO ₂ , Amorphous nanocrystals transform into TiO ₂ nanocrystals; 3D network nanoscale, Block-shaped TiO ₂ nanocrystals; wormlike, Convex | CA=4°; bandgap energy=2.58 eV; Hydrophilic, The degradation rate>70%; Photovoltaic efficiency≈0.016%~2.194%; Remove toxins; Reduce NO _x emission | photo-activities and Photocatalysis | [152-155] |

异的抗氧化性能，可广泛应用于高温环境中^[128]。此外，通过微弧氧化多层结构的设计和制备^[129-130]，调节涂层厚度、孔隙率、孔的大小分布等可获得高性能的热防护涂层，为高速飞行器、发动机热端部件等在高温下应用提供涂层体系与方法。

4.4 热控

航天器（卫星、空间站）的热控涂层，通过调节吸收率与发射率（吸辐比）调控温度范围，使电子器

件的工作温度维持在相对稳定的范围。人们通过设计微弧氧化涂层的组成与表面微纳孔结构（粗糙度）^[131-138]，从而调控太阳吸收率和发射率值（表 5 中 5-4）。因此，在保证涂层高表面质量的前提下，可适当调节电解液电导率，提高电流密度以及增加氧化时间，从而提高涂层厚度和表面粗糙度。针对高吸收发射比涂层，可同时提高太阳吸收率和发射率；针对低吸收发射比涂层，可降低太阳吸收率，提高发射率。此外，在电解液中添加阴、阳离子或纳米/微米颗粒，

或调控不同组分在微弧氧化涂层中的分布并形成不同的表面微纳孔结构, 对于改善涂层的吸收率和发射率也至关重要。涂层厚度、孔结构、孔尺寸和孔分布等调控对于热控性能的具体影响, 以及定量分析和模拟等, 还需要深入探究。

4.5 绝缘介电

轻合金作为电子器件防护外壳, 在高技术装备领域服役过程中, 需要具备电绝缘屏蔽性能, 以屏蔽外来干扰源, 使电子元器件避免损坏。微弧氧化技术在金属表面可以生成一层绝缘的氧化物膜, 但由于涂层表面疏松多孔, 含有大量的杂质, 且不同孔结构生长涂层的电绝缘性有较大差异, 因此需要在保证微弧氧化涂层高致密性的前提下, 提高涂层厚度, 降低孔隙率和缺陷, 从而提高涂层的电绝缘性(表 5 中 5-5) [139-141]。适当提高电解液的导电性, 可以增加陶瓷层厚度。利用富含硅酸盐的电解液, 可形成更厚、更致密的陶瓷层。初期采用高电流密度, 可形成致密性好的内层, 后期采用低电流密度, 可对多孔层的孔隙和缺陷进一步弥补和愈合。此外, 将电绝缘性高的纳米粒子添加到电解液^[139]中, 或进行封孔处理形成多层复合涂层, 可大幅度增加电绝缘性。

4.6 生物医用

钛、镁及其合金作为生物安全性良好的新一代医用金属材料, 被广泛关注, 然而表面无生物活性、与骨组织整合差、抗菌能力差、腐蚀降解调控能力有待提高等问题, 限制了其在临床上的扩大应用。微弧氧化涂层与金属植入手体以冶金结合, 而涂层含 Ca/P 等生物活性组分, 且表面存在微纳米多级孔结构, 为新生骨的长入提供了诱导能力(表 5 中 5-6)^[142]。同时, 微弧氧化在很多方面都具有可调控性, 包括: 调控微纳米分级孔结构, 促进细胞随孔长入, 提高生物相容性^[143]; 在涂层表面构建宏、介孔结构, 以匹配细胞粘附和骨组织生长^[144-146]; 调控表面成分及微纳结构, 改善表面生物活性与抑菌特性^[147], 减小与骨组织的力学失配程度; 提高镁合金的耐蚀性, 增强降解速度调控能力^[148-149]。此外, 通过工艺设计与热处理、水热处理、水汽处理、电沉积、等离子喷涂、溶胶凝胶、激光熔覆、磁控溅射、超声共聚等技术结合^[150-151], 获得多级微纳米孔结构的多层复合涂层。通过调节适合的孔隙率和特定的微纳米孔结构, 从而有效调控表面细胞与组织的附着行为, 并使其具有长期化学稳定性、抗菌、负载药物、细胞相容等多功能特性, 作为生物医学材料具有广阔的发展前景。

4.7 催化

微弧氧化涂层由于稳定性好、廉价、无毒、制备简单等优点, 在光催化领域受到广泛的关注。特别是在钛及钛合金表面制备与基体结合紧密的多孔可调

节的二氧化钛光催化膜层, 实现光催化剂的有效负载。在微弧氧化过程中, 通过调节电解液成分和电参数, 控制孔结构生长(孔隙率、孔尺寸、孔分布以及孔形貌), 并在孔壁上调控一些特殊结构(如纳米线、纳米棒、纳米团簇、纳米球以及具有高催化的微纳结构), 同时引入催化活性粒子 Tb、W、Co、Mn、Cu、Zn 等^[152-153], 可制备具有高催化活性的涂层(表 5 中 5-7)。另外, 可通过以微弧氧化为底层, 采用多步法、后处理等方式复合(表 5 中 5-7)^[154-155], 设计新颖结构, 并优化制备以 TiO₂ 为主要氧化物的多晶型复合物, 从而构建具有高催化活性的成分和结构的涂层, 为光催化应用提供涂层体系与方法。

4.8 探索新功能

微弧氧化涂层正在探索应用于新的领域, 如电磁屏蔽、活性电极、染料敏化太阳能电池等。G. LEE 等^[14]利用纳米粒子掺杂, 并结合微纳米孔的生长方式、分布情况、分级结构、比表面积等来调节涂层储存能量密度, 从而获得优异的容量和循环稳定性。Yang N. 等^[156]为了构建超高能量密度的超级电容器, 在钛板上利用微弧氧化及复合技术制备了多孔碳化钛/掺硼金刚石复合电极。微弧诱导促进了化学气相沉积过程中硼金刚石的生长, 制备出高性能的超级电容器(高的循环稳定性和能量密度)。Wen C. L. 等^[157]利用 CNTs 掺杂改性微弧氧化多孔涂层, 结合设计 Li⁺在微纳米结构中的扩散路径以及 CNTs 的导电性能, 明显增加了锂离子电池的容量, 扩大了电池功能化涂层在先进能源领域的应用。另外, 稀土掺杂的微弧氧化涂层具有良好的光致发光性能^[158-160], 充分利用了微弧氧化及复合涂层(过渡金属和稀土氧化物)的 PL 特性, 表现出广泛的应用前景。

5 结语

利用微弧氧化技术在金属及复合材料表面构建功能化陶瓷涂层, 已经显示出独特且不可替代的优势。功能化涂层的性能一定程度上取决于界面处、中间层及表面形成的微纳米孔及调控方式, 但微弧氧化瞬间放电特性难控制, 给不同种类微纳米孔的按需构建、消减(甚至消除)和利用带来巨大挑战。总体来说, 未来的发展重点在于以下几个方面:

1) 进一步揭示微纳米孔形成机理, 为精细调控提供方法指导。利用气体/等离子体的产生和扩散作用来研究介质击穿、“软”等离子体、发光现象以及等离子体温度的引发和增长; 从等离子体物理、电化学、电气工程、传输现象、热传导等方面, 获得等离子体放电对陶瓷层微纳米孔结构形成过程的影响因素; 结合计算机系统模拟计算等离子体能量、电子电流和电化学反应等来调节等离子体放电行为, 并与微纳米孔形成相关联。

2) 进一步探究不同类型微纳米孔的构建、消减(甚至消除)和利用的工艺方法,为涂层的功能性强化提供途径。从设计定制电源模式、调节电参数、电解液成分及浓度等方面,按需调控不同类型或特定尺寸的微纳米孔,以优化涂层结构和加强功能特性。

3) 进一步探究微纳米孔与涂层成分的协调控制方法及复合工艺调控方法,为新型功能化涂层的构建提供途径。在继续优化微纳米孔与涂层成分制备工艺,强化抗磨减摩、耐腐蚀、热防护、热控、绝缘、生物医学、催化等功能的基础上,通过微纳米粒子/离子/掺杂剂协调调控,或前处理与后处理复合工艺,构建多功能特性的新型涂层,来满足特殊服役环境的新应用(如电磁屏蔽、染料敏化太阳能电池及超级电容器等)。

参考文献:

- [1] XUE W, DENG Z, CHEN R, et al. Growth regularity of ceramic coatings formed by microarc oxidation on Al-Cu-Mg alloy[J]. Thin solid films, 2000, 372(1-2): 114-117.
- [2] RUDNEY V S, YAROVAYA T P, KON'SHIN V V, et al. Microplasma oxidation of an aluminum alloy in aqueous solutions containing sodium cyclohexa phosphate and nitrates of lanthanum and europium[J]. Russian journal of electrochemistry, 1998, 34(6): 510-516.
- [3] CUI L Y, ZENG R C, GUAN S K, et al. Degradation mechanism of micro-arc oxidation coatings on biodegradable Mg-Ca alloys: The influence of porosity[J]. Journal of alloys and compounds, 2017, 695: 2464-2476.
- [4] SHOKOHFAR M, ALLAHKARAM S R. Formation mechanism and surface characterization of ceramic composite coatings on pure titanium prepared by micro-arc oxidation in electrolytes containing nanoparticles[J]. Surface and coatings technology, 2016, 291: 396-405.
- [5] WANG Y M, JIANG B L, GUO L X, et al. Tribological behavior of microarc oxidation coatings formed on titanium alloys against steel in dry and solid lubrication sliding[J]. Applied surface science, 2006, 252(8): 2989-2998.
- [6] WANG Y M, WANG F H, XU M J, et al. Microstructure and corrosion behavior of coated AZ91 alloy by microarc oxidation for biomedical application[J]. Applied surface science, 2009, 255(22): 9124-9131.
- [7] GE Y L, WANG Y M, CHEN J C, et al. An Nb₂O₅-SiO₂-Al₂O₃/Nb₅Si₂/Nb₅Si₃ multilayer coating on Nb-Hf alloy to improve oxidation resistance[J]. Journal of alloys and compounds, 2018, 745: 271-281.
- [8] 张志莲, 张玉林, 陈飞. 氧化石墨烯对Mg-Li合金微弧氧化陶瓷层微观结构及耐蚀性的影响[J]. 表面技术, 2019, 48(6): 306-313.
- [9] AJITHKUMAR G, YOO B, GORAL D E, et al. Multimodal bioimaging using a rare earth doped Gd₂O₃: Yb/Er phosphor with upconversion luminescence and magnetic resonance properties[J]. J mater chem B, 2013, 1: 1561-1572.
- [10] TENG H P, HSU H W, LU F H. Formation of Ba_xSr_{1-x}TiO₃ films on TiN-coated substrates by plasma electrolytic oxidation[J]. Ceramics international, 2017, 43: S584-S590.
- [11] 陈姗姗, 顾桂松, 郭全忠, 等. 多孔镁表面微弧氧化涂层和氟化学转化涂层的对比研究[J]. 表面技术, 2021, 50(2): 13-21.
- [12] CHEN Shan-shan, GU Gui-song, GUO Quan-zhong, et al. Comparative study of micro-arc oxidation coating and fluorine-conversion coating on porous magnesium surface [J]. Surface technology, 2021, 50(2): 13-21.
- [13] ZHOU R, WEI D, CAO J, et al. Synergistic effects of surface chemistry and topologic structure from modified microarc oxidation coatings on Ti implants for improving osseointegration[J]. ACS applied materials & interfaces, 2015, 7(16): 8932-8941.
- [14] JIANG Y N, LIU B D, YANG W J, et al. New strategy for the in situ synthesis of single-crystalline MnWO₄/TiO₂ photocatalysts for efficient and cyclic photodegradation of organic pollutants[J]. Cryst eng comm, 2016, 18(10): 1832-1841.
- [15] LEE G, KIM S, KIM S, et al. SiO₂/TiO₂ composite film for high capacity and excellent cycling stability in lithium-ion battery anodes[J]. Advanced functional materials, 2017, 27(39): 1703538.
- [16] HAN Y, HONG S H, XU K. Structure and in vitro bioactivity of titania-based films by micro-arc oxidation[J]. Surface and coatings technology, 2003, 168(2-3): 249-258.
- [17] ZHANG Y M, BATAILLON-LINEZ P, HUANG P, et al. Surface analyses of micro-arc oxidized and hydrothermally treated titanium and effect on osteoblast behavior [J]. Journal of biomedical materials research part A, 2010, 68(2): 383-391.
- [18] HAN Y, HONG S H, XU K. Synthesis of nanocrystalline titania films by micro-arc oxidation[J]. Materials letters, 2002, 56(5): 744-747.
- [19] DONG Q, CHEN C, WANG D, et al. Research status about surface modification of biomedical Ti and its alloys by micro-arc oxidation[J]. Surface review and letters, 2008, 13(1): 35-43.
- [20] CURRAN J A, CLYNE T W. Porosity in plasma electrolytic oxide coatings[J]. Acta materialia, 2006, 54(7): 1985-1993.
- [21] KHAN R H U, YEROKHIN A, LI X, et al. Surface characterisation of DC plasma electrolytic oxidation treated 6082 aluminium alloy: Effect of current density and electrolyte concentration[J]. Surface and coatings technology, 2010, 205(6): 1679-1688.

- [21] SREEKANTH D, RAMESHBABU N, VENKATESWARLU K. Effect of various additives on morphology and corrosion behavior of ceramic coatings developed on AZ31 magnesium alloy by plasma electrolytic oxidation[J]. Ceramics international, 2012, 38(6): 4607-4615.
- [22] HUSSEIN R O, NIE X, NORTHWOOD D O. Influence of process parameters on electrolytic plasma discharging behaviour and aluminum oxide coating microstructure[J]. Surface and coatings technology, 2010, 205(6): 1659-1667.
- [23] YEROKHIN A L, VOEVODIN A A, LYUBIMOV V V, et al. Plasma electrolytic fabrication of oxide ceramic surface layers for tribotechnical purposes on aluminium alloys[J]. Surface and coatings technology, 1998, 110(3): 140-146.
- [24] 王亚明. Ti6Al4V 合金微弧氧化涂层的形成机制与摩擦学行为[D]. 哈尔滨: 哈尔滨工业大学, 2006.
- WANG Ya-ming. Formation mechanism and tribological behavior of microarc oxidation coating on Ti6Al4V alloy [D]. Harbin: Harbin Institute of Technology, 2006.
- [25] JIANG B L, WANG Y M. Plasma electrolytic oxidation treatment of aluminium and titanium alloys[M]. Cambridge: Woodhead Publishing, 2010: 110-154.
- [26] HONG F G, MAO Z A, SHEN X, et al. Effect of current density on mechanism of micro-arc oxidization and property of ceramic coating formed on magnesium alloys[J]. Rare metal materials and engineering, 2005, 34(10): 1554.
- [27] VIJH A K. Sparking voltages and side reactions during anodization of valve metals in terms of electron tunnelling[J]. Corrosion science, 1971, 11(6): 411-417.
- [28] IKONOPISOV S, GIRGINOV A, MACHKOVA M. Post-breakdown anodization of aluminium[J]. Electrochimica acta, 1977, 22(11): 1283-1286.
- [29] IKONOPISOV S. Theory of electrical breakdown during formation of barrier anodic films[J]. Electrochimica acta, 1977, 22(10): 1077-1082.
- [30] LI L H, KIM H W, LEE S H, et al. Biocompatibility of titanium implants modified by microarc oxidation and hydroxyapatite coating[J]. Journal of biomedical materials research part A, 2005, 73(1): 48.
- [31] KRYSMANN W, KURZE P, DITTRICH K H, et al. Process characteristics and parameters of anodic oxidation by spark discharge (ANOF)[J]. Crystal research and technology, 1984, 19(7): 973-979.
- [32] YEROKHIN A L, SNIZHKO L O, GUREVINA N L, et al. Discharge characterization in plasma electrolytic oxidation of aluminium[J]. Journal of physics D: Applied physics, 2003, 36(17): 2110.
- [33] 陈栋. 微弧氧化过程中裂纹和孔洞的形成方式及超声波影响的研究[D]. 秦皇岛: 燕山大学, 2018.
- CHEN Dong. Study on the formation mechanism of cracks and holes during micro-arc oxidation and the effects of ultrasonic waves[D]. Qinhuangdao: Yanshan University, 2018.
- [34] CLYNE T W, TROUGHTON S C. A review of recent work on discharge characteristics during plasma electrolytic oxidation of various metals[J]. International materials reviews, 2019, 64(3): 127-162.
- [35] WANG Y, LEI T, JIANG B, et al. Growth, microstructure and mechanical properties of microarc oxidation coatings on titanium alloy in phosphate-containing solution[J]. Applied surface science, 2004, 233(1-4): 258-267.
- [36] 王亚明, 邹永纯, 王树棋, 等. 金属微弧氧化功能陶瓷涂层设计制备与使役性能研究进展[J]. 中国表面工程, 2018, 31(4): 20-45.
- WANG Ya-ming, ZOU Yong-chun, WANG Shu-qi, et al. Design, fabrication and performance of multifunctional ceramic coatings formed by microarc oxidation on metals: A critical review[J]. China surface engineering, 2018, 31(4): 20-45.
- [37] HUSESEIN R O, NIE X, NORTHWOOD D O, et al. Spectroscopic study of electrolytic plasma and discharging behaviour during the plasma electrolytic oxidation (PEO) process[J]. Journal of physics D: Applied physics, 2010, 43(10): 105203.
- [38] CHENG Y L, XUE Z G, WANG Q, et al. New findings on properties of plasma electrolytic oxidation coatings from study of an Al-Cu-Li alloy[J]. Electrochim acta 2013, 107: 358-378.
- [39] LIU R, WU J, XUE W, et al. Discharge behaviors during plasma electrolytic oxidation on aluminum alloy[J]. Materials chemistry and physics, 2014, 148(1-2): 284-292.
- [40] 魏克俭, 薛文斌, 曲尧, 等. 镍微弧氧化表面处理技术研究进展[J]. 表面技术, 2019, 48(7): 11-23.
- WEI Ke-jian, XUE Wen-bin, QU Yao, et al. Advance in microarc oxidation surface treatment on Zr[J]. Surface technology, 2019, 48(7): 11-23.
- [41] JASPADR-MÉCUSON F, CZERWIEC T, HENRION G, et al. Tailored aluminium oxide layers by bipolar current adjustment in the Plasma Electrolytic Oxidation (PEO) process[J]. Surface and coatings technology, 2007, 201(21): 8677-8682.
- [42] MELHEM A, HENRION G, CZERWIEC T, et al. Changes induced by process parameters in oxide layers grown by the PEO process on Al alloys[J]. Surface and coatings technology, 2011, 205: 1363-1366.
- [43] KASEEM M, FATIMAH S, NASHRAH N, et al. Recent progress in surface modification of metals coated by plasma electrolytic oxidation: Principle, structure, and performance[J]. Progress in materials science, 2020, 117: 100735.
- [44] LI Y, WANG W, LIU H, et al. Formation and in vitro/in vivo performance of “cortex-like” micro/nano-structured TiO₂ coatings on titanium by micro-arc oxidation[J]. Materials science and engineering: C, 2018, 87: 90-103.
- [45] ZOU Y, WANG Y, WEI D, et al. In-situ SEM analysis of brittle plasma electrolytic oxidation coating bonded to plastic aluminum substrate: Microstructure and fracture behaviors[J]. Materials characterization, 2019, 156: 109851.

- [46] GUO H F, AN M Z, HUO H B, et al. Microstructure characteristic of ceramic coatings fabricated on magnesium alloys by micro-arc oxidation in alkaline silicate solutions [J]. *Applied surface science*, 2006, 252(22): 7911-7916.
- [47] RAKOCH A G, MONAKHOVA E P, KHABIBULLINA Z V, et al. Plasma electrolytic oxidation of AZ31 and AZ91 magnesium alloys: Comparison of coatings formation mechanism[J]. *Journal of magnesium and alloys*, 2020, 8(3): 587-600.
- [48] TROUGHTON S C, NOMINE A, DEAN J, et al. Effect of individual discharge cascades on the microstructure of plasma electrolytic oxidation coatings[J]. *Applied surface science*, 2016, 389: 260-269.
- [49] ZHANG X, ALIASGHARI S, NEMCOVA A, et al. X-ray computed tomographic investigation of the porosity and morphology of plasma electrolytic oxidation coatings[J]. *ACS applied materials and interfaces*, 2016, 8(13): 8801-8810.
- [50] LU X, BLAWERT C, TOLNAI D, et al. 3D reconstruction of plasma electrolytic oxidation coatings on Mg alloy via synchrotron radiation tomography[J]. *Corrosion science*, 2018, 139: 395-402.
- [51] NOMINE A, TROUGHTON S C, NOMINÉ A V, et al. High speed video evidence for localised discharge cascades during plasma electrolytic oxidation[J]. *Surface and coatings technology*, 2015, 269: 125-130.
- [52] CHENG Y, CAO J, PENG Z, et al. Wear-resistant coatings formed on Zircaloy-2 by plasma electrolytic oxidation in sodium aluminate electrolytes[J]. *Electrochimica acta*, 2014, 116: 453-466.
- [53] YANG X, CHEN L, QU Y, et al. Optical emission spectroscopy of plasma electrolytic oxidation process on 7075 aluminum alloy[J]. *Surface and coatings technology*, 2017, 324: 18-25.
- [54] ZOU Y, WANG Y, SUN Z, et al. Plasma electrolytic oxidation induced ‘local over-growth’ characteristic across substrate/coating interface: Effects and tailoring strategy of individual pulse energy[J]. *Surface and coatings technology*, 2018, 342: 198-208.
- [55] TIMOSHENKO A V, OPERA B K. Formation of protective wear-resistant oxide coatings on aluminum alloys by the micro plasma methods from aqueous electrolytes solutions[J]. *Proc international corrosion congress*, 1993, 1(12): 280-293.
- [56] SKELDON P, SHIMIZU K, THOMPSON G E. Selective interfacial processes and the incorporation of electrolyte species into anodic films on aluminum[J]. *Phil mag B*, 1995, 72(4): 391-400.
- [57] BROWN S D, KUNA K L, VAN T B. Anodic spark deposition from aqueous solutions of NaAlO_2 and Na_2SiO_3 [J]. *Journal of the American Ceramic Society*, 1971, 54(8): 384-390.
- [58] TCHERENENKO V I, SNEZHKO L A, PAPANOVA I I. Coatings by anodic spark electrolysis[M]. Leningrad: Khimiya, 1991.
- [59] LIU Z, WANG W, LIU H, et al. Formation and characterization of titania coatings with cortex-like slots formed on Ti by micro-arc oxidation treatment[J]. *Applied surface science*, 2013, 266: 250-255.
- [60] 孙乐, 马颖, 董海荣, 等. 硅酸钠在镁合金表面生成微弧氧化膜时的作用[J]. 稀有金属, 2020, 44(4): 378-386.
- SUN Le, MA Ying, DONG Hai-rong, et al. Role of sodium silicate for coating forming on magnesium alloys with microarc oxidation[J]. *Chinese journal of rare metals*, 2020, 44(4): 378-386.
- [61] 葛延峰, 蒋百灵, 时惠英. 硅酸钠浓度对铝合金微弧氧化起弧过程能量消耗的影响[J]. 中国有色金属学报, 2013, 23(4): 950-956.
- GE Yan-feng, JIANG Bai-ling, SHI Hui-ying. Effect of Na_2SiO_3 concentration on energy consumption during arcing process of micro-arc oxidation on aluminum alloys[J]. *The Chinese journal of nonferrous metals*, 2013, 23(4): 950-956.
- [62] 但敏, 童洪辉, 沈丽如, 等. 六偏磷酸钠对 LD7 铝合金微弧氧化陶瓷膜结构及耐腐蚀性能的改善作用[J]. 材料保护, 2011, 44(5): 11-13.
- DAN Min, TONG Hong-hui, SHEN Li-ru, et al. The effect of sodium hexametaphosphate on the structure and corrosion resistance of LD7 aluminum alloy micro-arc oxidation ceramic film[J]. *Materials protection*, 2011, 44(5): 11-13.
- [63] 李建中, 邵忠财, 田彦文, 等. 不同含磷电解液在微弧氧化过程中的作用[J]. 中国腐蚀与防护学报, 2004, 24(4): 222-225.
- LI Jian-zhong, SHAO Zhong-cai, TIAN Yan-wen, et al. The action of the forms of P element on the process of the microarc oxidation[J]. *Journal of Chinese Society for Corrosion and Protection*, 2004, 24(4): 222-225.
- [64] 方健亮, 吴青, 于有相, 等. 偏铝酸钠对铝基复合材料表面微弧氧化膜性能的影响[J]. 电镀与环保, 2020, 40(3): 57-59.
- FANG Jian-liang, WU Qing, YU You-xiang, et al. Effect of sodium metaluminate on properties of micro-arc oxidation coatings on surface of aluminum matrix composites [J]. *Electroplating and pollution control*, 2020, 40(3): 57-59.
- [65] 薛文斌, 邓志威, 李永良, 等. Ti-6Al-4V 在 NaAlO_2 溶液中微弧氧化陶瓷膜的组织结构研究[J]. 材料科学与工艺, 2000(3): 41-45.
- XUE Wen-bin, DENG Zhi-wei, LI Yong-liang, et al. Microstructure of ceramic coatings formed on Ti-6Al-4V alloy by microarc oxidation in NaAlO_2 solution[J]. *Materials science and technology*, 2000(3): 41-45.
- [66] WANG S, WANG Y, CUI Y, et al. High voltage resistance ceramic coating fabricated on titanium alloy for insulation shielding application[J]. *Ceramics international*, 2019, 45(2): 1909-1917.
- [67] 曹雅心, 王梦杰, 周凡, 等. KOH 浓度对 LA103Z 镁锂

- 合金微弧氧化成膜过程及膜层耐蚀性的影响[J]. 表面技术, 2021, 50(3): 348-355.
- CAO Ya-xin, WANG Meng-jie, ZHOU Fan, et al. Effect of KOH concentration on the growth process and corrosion resistance of micro-arc oxidation (MAO) coatings on LA103Z Mg-Li alloy[J]. Surface technology, 2021, 50(3): 348-355.
- [68] LI Y, WANG W, YU F, et al. Characterization and cytocompatibility of hierarchical porous TiO₂ coatings incorporated with calcium and strontium by one-step micro-arc oxidation[J]. Materials science and engineering: C, 2020, 109: 110610.
- [69] GUAN S, QI M, LI Y, et al. Morphology evolution of the porous coatings on Ti-xAl alloys by Al adding into Ti during micro-arc oxidation in Na₂B₄O₇ electrolyte[J]. Surface and coatings technology, 2020, 395: 125948.
- [70] 段关文, 高晓菊, 满红, 等. 微弧氧化研究进展[J]. 兵器材料科学与工程, 2010, 33(5): 102-106.
- DUAN Guan-wen, GAO Xiao-ju, MAN Hong, et al. Research progress in micro-arc oxidation[J]. Ordnance material science and engineering, 2010, 33(5): 102-106.
- [71] VENKATESWARLU K, RAMESHBABU N, SREEKA-NTH D, et al. Role of electrolyte chemistry on electronic and in vitro electrochemical properties of micro-arc oxidized titania films on Cp Ti[J]. Electrochimica acta, 2013, 105: 468-480.
- [72] SIMCHEN F, SIEBER M, LAMPEK T. Electrolyte influence on ignition of plasma electrolytic oxidation processes on light metals[J]. Surface and coatings technology, 2017, 315: 205-213.
- [73] ROGOV A B, SHAYAPOV V R. The role of cathodic current in PEO of aluminum: influence of cationic electrolyte composition on the transient current-voltage curves and the discharges optical emission spectra[J]. Applied surface science, 2017, 394: 323-332.
- [74] ZHANG D Z, ZHOU Y C, WEN L, et al. Liquid-phase plasma assisted electrophoresis and sintering SiC/hBN nanocomposite ceramic coating on aluminum alloy for radiative heat dissipation[J]. Ceramics international, 2021, 47(7): 9310-9316.
- [75] WANG Y Q, WANG X J, GONG W X, et al. Effect of SiC particles on microarc oxidation process of magnesium matrix composites[J]. Applied surface science, 2013, 283(15): 906-913.
- [76] CHEN G L, WANG Y M, ZHOU Y C, et al. Hexagonal boron nitride and alumina dual-layer coating for space solar thermal shielding[J]. Chemical engineering journal, 2021, 421: 127802.
- [77] WANG S Q, WANG Y M, CHEN J C, et al. Simple and scalable synthesis of super-repellent multilayer nanocomposite coating on Mg alloy with mechanochemical robustness, high temperature endurance and electric protection [J/OL]. Journal of magnesium alloys, 2021-02-25. <https://doi.org/10.1016/j.jma.2020.11.024>.
- [78] BOLSHENKO A V, PAVLENKO A V, PUZIN V S, et al. Power supplies for microarc oxidation devices[J]. Life sci j, 2014, 11: 263-268.
- [79] YANG W, ZHAO Y, YANG S. Effects of characteristic and parameters of power supply on micro-arc oxidation coatings property and energy consumption[J]. Journal of materials engineering, 2010(2): 86-90.
- [80] YEROKHIN A L, SHATROV A, SAMSONOV V, et al. Oxide ceramic coatings on aluminium alloys produced by a pulsed bipolar plasma electrolytic oxidation process[J]. Surface and coatings technology, 2005, 199(2-3): 150-157.
- [81] WANG Y, JIANG B, LEI T, et al. Dependence of growth features of microarc oxidation coatings of titanium alloy on control modes of alternate pulse[J]. Materials letters, 2004, 58(12-13): 1907-1911.
- [82] CHENG Y, WANG T, LI S, et al. The effects of anion deposition and negative pulse on the behaviours of plasma electrolytic oxidation (PEO)—A systematic study of the PEO of a zirlo alloy in aluminate electrolytes[J]. Electrochimica acta, 2017, 225: 47-68.
- [83] ROGOV A B, YEROKHIN A, MATTHEWS A. The role of cathodic current in plasma electrolytic oxidation of aluminum: Phenomenological concepts of the “soft sparking” mode[J]. Langmuir, 2017, 33: 11059-11069.
- [84] TSAI D S, CHOU C C. Review of the soft sparking issues in plasma electrolytic oxidation[J]. Metals, 2018, 8: 105.
- [85] WANG Y M, JIA D C, GUO L X, et al. Effect of discharge pulsating on microarc oxidation coatings formed on Ti6Al4V alloy[J]. Materials chemistry and physics, 2005, 90(1): 128-133.
- [86] 李响, 姚忠平, 李雪健, 等. 微弧氧化技术在热控涂层中的应用[J]. 表面技术, 2019, 48(7): 24-36.
- LI Xiang, YAO Zhong-ping, LI Xue-jian, et al. Application of micro-arc oxidation technology in thermal control coating[J]. Surface technology, 2019, 48(7): 24-36.
- [87] HORNBERGER H, VIRTANEN S, BOCCACCINI A R. Biomedical coatings on magnesium alloys—A review[J]. Acta biomaterialia, 2012, 8(7): 2442-2455.
- [88] GEETHA M, SINGH A K, ASOKAMANI R, et al. Ti based biomaterials, the ultimate choice for orthopaedic implants—A review[J]. Progress in materials science, 2009, 54(3): 397-425.
- [89] WEI D, ZHOU Y, YANG C. Characteristic and microstructure of the microarc oxidized TiO₂-based film containing P before and after chemical and heat treatment[J]. Applied surface science, 2009, 255(18): 7851-7857.
- [90] JIANG Y, LIU B, YANG W, et al. Crystalline (Ni_{1-x}Co_x)₂TiO₇ nanostructures grown in situ on a flexible metal substrate used towards efficient CO oxidation[J]. Nanoscale, 2017, 9: 11713.
- [91] ZHAO L, CUI C, WANG Q, et al. Growth characteristics and corrosion resistance of micro-arc oxidation coating on pure magnesium for biomedical applications[J]. Corrosion

- science, 2010, 52(7): 2228-2234.
- [92] ZHANG P, ZUO Y. Relationship between porosity, pore parameters and properties of microarc oxidation film on AZ91D magnesium alloy[J]. Results in physics, 2019, 12: 2044-2054.
- [93] LARSON C, SMITH J R, ARMSTRONG G J. Current research on surface finishing and coatings for aerospace bodies and structures—A review[J]. Transactions of the IMF, 2013, 91(3): 120-132.
- [94] WANG Y H, LIU Z G, OUYANG J H, et al. Influence of electrolyte compositions on structure and high-temperature oxidation resistance of microarc oxidation coatings formed on Ti₂AlNb alloy[J]. Journal of alloys and compounds, 2015, 647: 431-437.
- [95] 沈德久, 廖波, 王玉林, 等. 影响铝微弧氧化陶瓷层电绝缘性的工艺因素探讨[J]. 材料开发与应用, 2002, 17(4): 22-23.
- SHEN De-jiu, LIAO Bo, WANG Yu-Lin, et al. Effect of technological factors on electric insulance of micro-arc oxidized ceramic coat on aluminium[J]. Material development and application, 2002, 17(4): 22-23.
- [96] LEE K M, KIM Y S, YANG H W, et al. Formation of ZrO₂ in coating on Mg-3wt.%Al-1wt.%Zn alloy via plasma electrolytic oxidation: Phase and structure of zirconia [J]. Materials characterization, 2015, 99: 101-108.
- [97] LIU F, SHAN D Y, SONG Y W, et al. Formation process of composite plasma electrolytic oxidation coating containing zirconium oxides on AM50 magnesium alloy[J]. Transactions of Nonferrous Metals Society of China, 2011, 21(4): 943-948.
- [98] LU X P, MOHEDANO M, BLAWERT C, et al. Plasma electrolytic oxidation coatings with particle additions—A review[J]. Surface and coatings technology, 2016(307): 1165-1182.
- [99] 王亚明, 邹永纯, 王树棋, 等. 一种改性的金属材料及金属表面的改性方法: 中国, CN110195248A[P]. 2019-09-03.
- WANG Ya-ming, ZOU Yong-chun, WANG Shu-qи, et al. A modified metal material and metal surface modification method: China, CN110195248A[P]. 2019-09-03.
- [100] 王亚明, 王树棋, 邹永纯, 等. 一种钛表面超疏水复合涂层及其制备方法: 中国, CN111455429A[P]. 2020-07-28.
- WANG Ya-ming, WANG Shu-qи, ZOU Yong-chun, et al. A superhydrophobic composite coating on titanium surface and its preparation method: China, CN111455429A [P]. 2020-07-28.
- [101] CHERNYKH I V, LUKIYANCHUK I V, RUDNEV V S, et al. Silicate coatings on titanium, modified with transition metal oxides and their activity in CO oxidation[J]. Russian journal of applied chemistry, 2013, 86(3): 319-325.
- [102] ZHANG G, WU L, TANG A, et al. Active corrosion protection by a smart coating based on a MgAl-layered double hydroxide on a cerium-modified plasma electrolytic oxidation coating on Mg alloy AZ31[J]. Corrosion science, 2018, 139: 370-382.
- [103] GU Y, BANDOPADHYAY S, CHEN C, et al. Long-term corrosion inhibition mechanism of microarc oxidation coated AZ31 Mg alloys for biomedical applications[J]. Materials and design, 2013, 46: 66-75.
- [104] LU X, BLAWERT C, ZHELUDKEVICH M L, et al. Insights into plasma electrolytic oxidation treatment with particle addition[J]. Corrosion science, 2015, 101: 201-207.
- [105] LALEH M, KARGAR F, ROUHAGHDAM A S. Investigation of rare earth sealing of porous micro-arc oxidation coating formed on AZ91D magnesium alloy[J]. Journal of rare earths, 2012, 30(12): 1293-1297.
- [106] BARIK R C, WHARTON J A, WOOD R J K, et al. Corrosion, erosion and erosion-corrosion performance of Plasma Electrolytic Oxidation (PEO) deposited Al₂O₃ coatings[J]. Surface and coatings technology, 2005, 199(2-3): 158-167.
- [107] NAZEER A A, AL-HETLANI E, AMIN M O, et al. A poly (butyl methacrylate)/graphene oxide/TiO₂ nanocomposite coating with superior corrosion protection for AZ31 alloy in chloride solution[J]. Chemical engineering journal, 2019, 361: 485-498.
- [108] WANG Z W, WANG Y M, LIU Y, et al. Microstructure and infrared emissivity property of coating containing TiO₂ formed on titanium alloy by microarc oxidation[J]. Current applied physics, 2011, 11(6): 1405-1409.
- [109] LI B, HAN Y, QI K. Formation mechanism, degradation behavior, and cytocompatibility of a nanorod-shaped HA and pore-sealed MgO bilayer coating on magnesium[J]. ACS applied materials and interfaces, 2014, 6(20): 18258-18274.
- [110] PENG F, WANG D, TIAN Y, et al. Sealing the pores of PEO coating with Mg-Al layered double hydroxide: Enhanced corrosion resistance, cytocompatibility and drug delivery ability[J]. Scientific reports, 2017, 7(1): 1-12.
- [111] LUKIYANCHUK I V, CHERNYKH I V, RUDNEV V S, et al. Silicate coatings on titanium modified by cobalt and/or copper oxides and their activity in CO oxidation[J]. Protection of metals and physical chemistry of surfaces, 2015, 51(3): 448-457.
- [112] CUI L Y, GAO S D, LI P P, et al. Corrosion resistance of a self-healing micro-arc oxidation/polymethyltrimethoxysilane composite coating on magnesium alloy AZ31[J]. Corrosion science, 2017, 118: 84-95.
- [113] CHEN F, YU P, ZHANG Y. Healing effects of LDHs nanoplatelets on MAO ceramic layer of aluminum alloy[J]. Journal of alloys and compounds, 2017, 711: 342-348.
- [114] STOGADINOVIĆ S, TADIĆ N, RADIĆ N, et al. Effect of Tb³⁺ doping on the photocatalytic activity of TiO₂ coatings formed by plasma electrolytic oxidation of titanium [J]. Surface and coatings technology, 2018, 337: 279-289.
- [115] WANG Y M, JIANG B L, LEI T Q, et al. Microarc oxidation coatings formed on Ti6Al4V in Na₂SiO₃ system sol-

- ution: Microstructure, mechanical and tribological properties[J]. Surface and coatings technology, 2006, 201(1-2): 82-89.
- [116] CAI R, ZHAO C, NIE X. Effect of plasma electrolytic oxidation process on surface characteristics and tribological behavior[J]. Surface and coatings technology, 2019, 375: 824-832.
- [117] TRAN Q P, CHIN T S, KUO Y C, et al. Diamond powder incorporated oxide layers formed on 6061 Al alloy by plasma electrolytic oxidation[J]. Journal of alloys and compounds, 2018, 751: 289-298.
- [118] CHEN Y, LU X, BLAWERT C, et al. Formation of self-lubricating PEO coating via in-situ incorporation of PTFE particles[J]. Surface and coatings technology, 2018, 337: 379-388.
- [119] LU X, BLAWERT C, HUANG Y, et al. Plasma electrolytic oxidation coatings on Mg alloy with addition of SiO₂ particles[J]. Electrochimica acta, 2016, 187: 20-33.
- [120] AO N, LIU D, WANG S, et al. Microstructure and tribological behavior of a TiO₂/hBN composite ceramic coating formed via micro-arc oxidation of Ti-6Al-4V alloy[J]. Journal of materials science & technology, 2016, 32(10): 1071-1076.
- [121] 周科, 王树棋, 娄霞, 等. TA15 合金微弧氧化陶瓷涂层制备与电偶腐蚀性能[J]. 表面技术, 2019, 48(7): 72-80.
ZHOU Ke, WANG Shu-qí, LOU Xia, et al. Preparation and galvanic corrosion resistance of microarc oxidation ceramic coatings on TA15 alloy[J]. Surface technology, 2019, 48(7): 72-80.
- [122] GUO X, DU K, GUO Q, et al. Experimental study of corrosion protection of a three-layer film on AZ31B Mg alloy[J]. Corrosion science, 2012, 65: 367-375.
- [123] QIU Z, WANG R, WU J, et al. Graphene oxide as a corrosion-inhibitive coating on magnesium alloys[J]. RSC advances, 2015, 5(55): 44149-44159.
- [124] WEN L, WANG Y, ZHOU Y, et al. Microstructure and corrosion resistance of modified 2024Al alloy using surface mechanical attrition treatment combined with micro-arc oxidation process[J]. Corrosion science, 2011, 53(1): 473-480.
- [125] WANG S Q, WANG Y M, ZOU Y C, et al. Scalable-manufactured superhydrophobic multilayer nanocomposite coating with mechanochemical robustness and high-temperature endurance[J]. ACS applied materials and interfaces, 2020, 12(31): 35502-35512.
- [126] FARHADI S S, ALIOFKHAZRAEI M, DARBand G B, et al. Wettability and corrosion behavior of chemically modified plasma electrolytic oxidation nanocomposite coating[J]. Journal of materials engineering and performance, 2017, 26(10): 4797-4806.
- [127] ARUNNELLALAIAPPAN T, ASHFAQ M, KRISHNA L R, et al. Fabrication of corrosion-resistant Al₂O₃-CeO₂ composite coating on AA7075 via plasma electrolytic oxidation coupled with electrophoretic deposition[J]. Ceramics international, 2016, 42(5): 5897-5905.
- [128] CURRAN J A, KALKANCI H, MAGUROVA Y, et al. Mullite-rich plasma electrolytic oxide coatings for thermal barrier applications[J]. Surface and coatings technology, 2007, 201(21): 8683-8687.
- [129] GE Y L, WANG Y M, CHEN J C, et al. Hot corrosion behavior of NbSi₂/SiO₂-Nb₂O₅ multilayer coating on Nb alloy[J]. Journal of alloys and compounds, 2018, 767: 7-15.
- [130] DU W, ZHANG S, LUO X, et al. In-situ reaction synthesis of composite coating on titanium alloy for improving high temperature oxidation resistance[J]. Journal of alloys and compounds, 2017, 729: 970-977.
- [131] DING Z Y, WANG Y H, OUYANG J H, et al. Insights into structure and high-temperature oxidation behavior of plasma electrolytic oxidation ceramic coatings formed in NaAlO₂-Na₂CrO₄ electrolyte[J]. Journal of materials science, 2018, 53(14): 9978-9987.
- [132] CHEN G, WANG Y, ZOU Y, et al. A fractal-patterned coating on titanium alloy for stable passive heat dissipation and robust superhydrophobicity[J]. Chemical engineering journal, 2019, 374: 231-241.
- [133] ZOU Y, WANG Y, XU S, et al. Superhydrophobic double-layer coating for efficient heat dissipation and corrosion protection[J]. Chemical engineering journal, 2019, 362: 638-649.
- [134] WANG L, ZHOU J, LIANG J, et al. Thermal control coatings on magnesium alloys prepared by plasma electrolytic oxidation[J]. Applied surface science, 2013, 280: 151-155.
- [135] GE Y L, WANG Y M, ZHANG Y F, et al. The improved thermal radiation property of SiC doped microarc oxidation ceramic coating formed on niobium metal for metal thermal protective system[J]. Surface and coatings technology, 2017, 309: 880-886.
- [136] YAO Z P, HU B, SHEN Q X, et al. Preparation of black high absorbance and high emissivity thermal control coatings on Ti alloys by plasma electrolytic oxidation[J]. Surface and coatings technology, 2014, 253: 166-170.
- [137] LI H, LU S T, QIN W, et al. In-situ grown MgO-ZnO ceramic coating with high thermal emittance on Mg alloy by plasma electrolytic oxidation[J]. Acta astronautica, 2017, 136: 230-235.
- [138] ZOU Y, WANG Y, WEI D, et al. Facile one-step fabrication of multilayer nanocomposite coating for radiative heat dissipation[J]. ACS applied electronic materials, 2019, 1(8): 1527-1537.
- [139] WANG S Q, WANG Y M, ZOU Y C, et al. A self-adjusting PTFE/TiO₂ hydrophobic double-layer coating for corrosion resistance and electrical insulation[J]. Chemical engineering journal, 2020, 402: 126116.
- [140] 何翔, 熊梦颖. 铝合金表面陶瓷化及绝缘性能研究[J]. 兵器材料科学与工程, 2013, 36(1): 39-42.

- HE Xiang, XIONG Meng-ying. Preparation and insulating property of ceramic coating on aluminum alloy surface[J]. Ordnance material science and engineering, 2013, 36(1): 39-42.
- [141] WANG M, ZHANG G, LI W, et al. Microstructure and properties of BaTiO₃ ferroelectric films prepared by DC micro arc oxidation[J]. Bulletin of the Korean Chemical Society, 2015, 36(4): 1178-1182.
- [142] WEI D, ZHOU Y, JIA D, et al. Effect of heat treatment on the structure and in vitro bioactivity of microarc-oxidized (MAO) titania coatings containing Ca and P ions[J]. Surface and coatings technology, 2007, 201(21): 8723-8729.
- [143] ZHOU R, WEI D, CHENG S, et al. Structure, MC3T3-E1 cell response, and osseointegration of macroporous titanium implants covered by a bioactive microarc oxidation coating with microporous structure[J]. ACS applied materials and interfaces, 2014, 6(7): 4797-4811.
- [144] WEI D, ZHOU Y, YANG C. Structure, cell response and biomimetic apatite induction of gradient TiO₂-based/nano-scale hydrophilic amorphous titanium oxide containing Ca composite coatings before and after crystallization[J]. Colloids and surfaces B: Biointerfaces, 2009, 74(1): 230-237.
- [145] WANG Y M, GUO J W, ZHUANG J P, et al. Development and characterization of MAO bioactive ceramic coating grown on micro-patterned Ti6Al4V alloy surface [J]. Applied surface science, 2014, 299: 58-65.
- [146] 魏大庆. Ti6Al4V 表面微弧氧化生物涂层结构修饰与磷灰石形成动力学[D]. 哈尔滨: 哈尔滨工业大学, 2008.
WEI Da-qing. Structural modification and kinetics for the apatite formation of the microarc oxidation biocoatings on Ti6AL4V[D]. Harbin: Harbin Institute of Technology, 2008.
- [147] DU Q, WEI D, LIU S, et al. The hydrothermal treated Zn-incorporated titania based microarc oxidation coating: Surface characteristics, apatite-inducing ability and antibacterial ability[J]. Surface and coatings technology, 2018, 352: 489-500.
- [148] WU Y, WANG Y, TIAN S, et al. Formation mechanism, degradation behavior, and cytocompatibility of a double-layered structural MAO/rGO-CaP coating on AZ31 Mg [J]. Colloids and surfaces B: Biointerfaces, 2020, 190: 110901.
- [149] WU Y F, WANG Y M, JING Y B, et al. In vivo study of microarc oxidation coated biodegradable magnesium plate to heal bone fracture defect of 3 mm width[J]. Colloids and surfaces B: Biointerfaces, 2017, 158: 147-156.
- [150] LI G, CAO H, ZHANG W, et al. Enhanced osseointegration of hierarchical micro/nanotopographic titanium fabricated by microarc oxidation and electrochemical treatment[J]. ACS applied materials and interfaces, 2016, 8(6): 3840-3852.
- [151] ZHOU J, LI B, LU S, et al. Regulation of osteoblast proliferation and differentiation by interrod spacing of Sr-HA nanorods on microporous titania coatings[J]. ACS applied materials and interfaces, 2013, 5(11): 5358-5365.
- [152] BAYATI M R, MOLAEI R, ZARGAR H R, et al. A facile method to grow V-doped TiO₂ hydrophilic layers with nano-sheet morphology[J]. Materials letters, 2010, 64(22): 2498-2501.
- [153] LUKIYANCHUK I V, CHERNYKH I V, RUDNEV V S, et al. Silicate coatings on titanium modified by cobalt and/or copper oxides and their activity in CO oxidation[J]. Protection of metals and physical chemistry of surfaces, 2015, 51(3): 448-457.
- [154] CHU P J, WU S Y, CHEN K C, et al. Nano-structured TiO₂ films by plasma electrolytic oxidation combined with chemical and thermal post-treatments of titanium, for dye-sensitised solar cell applications[J]. Thin solid films, 2010, 519(5): 1723-1728.
- [155] AL Z W, KIM M J, YOON D K, et al. Effect of organic compounds and rough inorganic layer formed by plasma electrolytic oxidation on photocatalytic performance[J]. Journal of alloys and compounds, 2020, 823: 153787.
- [156] XU J, YANG N, HEUSER S, et al. Achieving ultrahigh energy densities of supercapacitors with porous titanium carbide/boron-doped diamond composite electrodes[J]. Advanced energy materials, 2019, 9(17): 1803623.
- [157] LO W C, SU S H, CHU H J, et al. TiO₂-CNTs grown on titanium as an anode layer for lithium-ion batteries[J]. Surface and coatings technology, 2018, 337: 544-551.
- [158] ZOLOTARJOVS A, SMITS K, KRUMINA A, et al. Luminescent PEO coatings on aluminum[J]. ECS journal of solid state science and technology, 2016, 5: 150-153.
- [159] RUBIO E J, ATUCHIN V V, KRUCHININ V N, et al. Electronic structure and optical quality of nanocrystalline Y₂O₃ film surfaces and interfaces on silicon[J]. Journal of physical chemistry C, 2014, 118: 13644-13651.
- [160] ĆIRIĆ A, STOJADINOVIĆ S. Photoluminescence of Gd₂O₃ and Gd₂O₃:Ln³⁺ (Ln=Eu, Er, Ho) formed by plasma electrolytic oxidation of pure gadolinium substrate[J]. Optical material, 2020, 99: 109546.